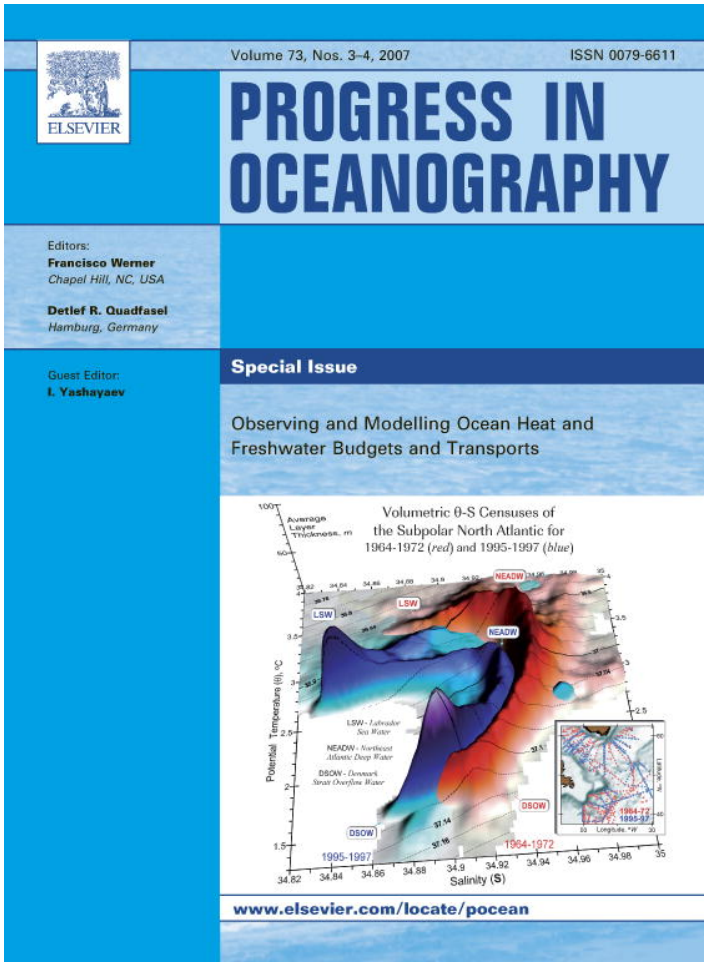

Available online at www.sciencedirect.com
ScienceDirect
Progress in Oceanography 73 (2007) 384–405
Progress in Oceanography
www.elsevier.com/locate/pocean

Causes of a fresher, colder northern North Atlantic in late 20th century in a coupled model

Aixue Hu [a,*], Gerald A. Meehl [a], Weiqing Han [b]

[a] *Climate and Global Dynamics Division, National Center for Atmospheric Research, Boulder, CO 80305, USA*
[b] *Department of Atmospheric and Oceanic Sciences, University of Colorado, Boulder, CO 80309, USA*

Accepted 29 July 2006
Available online 21 April 2007

Abstract

Observational evidence indicates that in the northern North Atlantic, especially in the Labrador Sea, almost the whole column of the ocean water is fresher, and colder in late 20th century than in 1950–1960s. Here we analyze a four-member ensemble of the 20th century simulations from a coupled climate model to examine the possible causes for these observed changes. The model simulations resemble the observed changes in the northern North Atlantic. The simulated results show that a decreased meridional freshwater divergence and an increased meridional heat divergence associated with a weaker thermohaline circulation in the North Atlantic are the primary causes for the freshening and cooling in the northern North Atlantic. The increased precipitation less evaporation tends to enforce the freshening, but the reduced sea ice flux into this region tends to weaken it. On the other hand, the surface warming induced by a higher atmospheric CO_2 concentration tends to heat up the northern North Atlantic, but is overcome by the cooling from increased meridional heat divergence.

Keywords: Meridional freshwater transport; Meridional heat transport; Thermohaline circulation

1. Introduction

In recent observational studies (e.g., Antonov et al., 2002; Dickson et al., 2002; Curry et al., 2003; Levitus et al., 2005a,b; Boyer et al., 2005; Antonov et al., 2005), the northern North Atlantic ocean is found to be undergoing remarkable changes – namely a trend of freshening, and cooling of the whole water column especially in the Labrador Sea (see Fig. 2b and c in Curry et al., 2003) and also in the northern North Atlantic between about 45° to 65°N in the late 20th century relative to the mid-20th century (see Fig. A6 in Levitus et al., 2005a; and Fig. 1a in Boyer et al., 2005). Dickson et al. (2002) examined the water mass property changes of the North Atlantic overflow system at several key pathways. Their evidence shows a freshening trend of the Denmark Strait Overflow water (DSOW) and the Faroe Bank overflow water. These overflow waters along with the dense water formed in the Labrador Sea (the Labrador Sea Water) feed into the lower

* Corresponding author. Tel.: +1 303 497 1334; fax: +1 303 497 1348.
E-mail address: ahu@ucar.edu (A. Hu).

0079-6611/$ - see front matter
doi:10.1016/j.pocean.2006.07.008

branch of the global scale oceanic circulation – the thermohaline circulation (THC). Curry et al. (2003) studied the observed temperature and salinity changes along a specific cross-section in the Atlantic from 60°N to 50°S. They further demonstrate a freshening and cooling in the Labrador Sea from the surface to about 2500 m deep, and also show a decrease in upper ocean density. Antonov et al. (2002) analyzed the heat and salt effects on steric sea level changes during 1957–1994. They found a cooling and freshening of the upper 3000 m ocean in the entire northern North Atlantic in 1978–1994 relative to the mean state of 1948–1996. Levitus et al. (2005a) and Boyer et al. (2005) studied the trend of zonal mean temperature and salinity change between 1955–1959 and 1994–1998 in the Atlantic. The patterns of zonal mean temperature and salinity anomalies are similar to those of Curry et al. (2003), and their conclusions are consistent with Antonov et al. (2002).

The thermohaline circulation is a global scale three-dimensional circulation which plays a key role in redistributing heat and freshwater meridionally. Changes in THC may result in significant regional (such as Europe) and global climate change (e.g., Cubasch et al., 2001; Stouffer et al., 2006). From the observations, it is very hard to link the observed water property changes in the northern North Atlantic to the THC, owing to the inability to derive the time-evolving THC from available observed ocean data. However, the freshening is a sign of increased freshwater supply to the subpolar ocean and may have resulted in a more stabilized upper ocean. On the other hand, the surface cooling in the same region has a compensative effect on the changes of the surface density, for example, surface cooling would induce a surface density increase and surface freshening would induce a surface density decrease. As shown in Fig. 3f of this paper, the surface density decreases in some parts of the northern North Atlantic region, but increases in other parts. Due to the fact that the deep convection occurs in very localized regions, it is difficult to conclude whether the THC or the North Atlantic deep water (NADW) formation has decreased or not from the available observations in this region. However, a recent study of the meridional transport at 25°N in the Atlantic indicates that the THC might have weakened by up to 30% since the 1950s (Bryden et al., 2005).

Possible reasons for the observed freshening and cooling in the northern North Atlantic have been attributed to a combined effect of freshwater export from the Arctic in the form of ice and melt-water, increased net precipitation, increased continental runoff and the severe winters in the early 1980 s and 1990s in the Labrador Sea (Abdalati and Steffen, 1997; Dickson et al., 2000; Vinje, 2001; Peterson et al., 2002; Belkin et al., 1998; Josey and Marsh, 2005), and may also be related to the upward trend of the North Atlantic Oscillation (NAO) during the second half of the 20th century (Dickson et al., 1996). The lack of systematic long-term observed data makes it difficult to attribute the relative importance of each of those potential contributors to the observed changes in the northern North Atlantic.

Here, we utilize a global coupled model, the Parallel Climate Model (PCM), to study the relative importance of these contributors to the recent observed freshening and cooling in the subpolar North Atlantic and the relationship between the observed changes and the THC. Our model results show an enhanced precipitation less evaporation (P–E, hereafter) in the polar–sub-polar North Atlantic, but a reduction of sea ice export from the Arctic to the Greenland–Iceland–Norwegian (GIN) Seas and further into Labrador Sea. The combined effect of these two fresh water sources is a small increase in net surface fresh water input into the GIN Seas and a small decrease in the Labrador Sea and south of Denmark Strait region (SDSR, hereafter. See Fig. 1 for a geographic map). The net surface heat fluxes in both the Labrador Sea and SDSR exhibit a decrease in heat loss, which contradict the cooling in the water column. On the other hand, the divergence of the meridional freshwater transport between 45° and 65°N is decreased, resulting in a net increase in freshwater supply in that water column. Additionally, the increased divergence of meridional heat transport in the same region leads to a higher heat loss in that water column. The changes in meridional heat and freshwater divergence are closely linked to a weaker THC in our model which highlights the importance of the relationship between the subpolar freshening, cooling and changes in the THC.

2. Model and experiments

2.1. Model

The parallel climate model (PCM) is a fully coupled climate model with no flux adjustment as described in detail by Washington et al. (2000). PCM consists of four component models: atmosphere, ocean, land, and sea

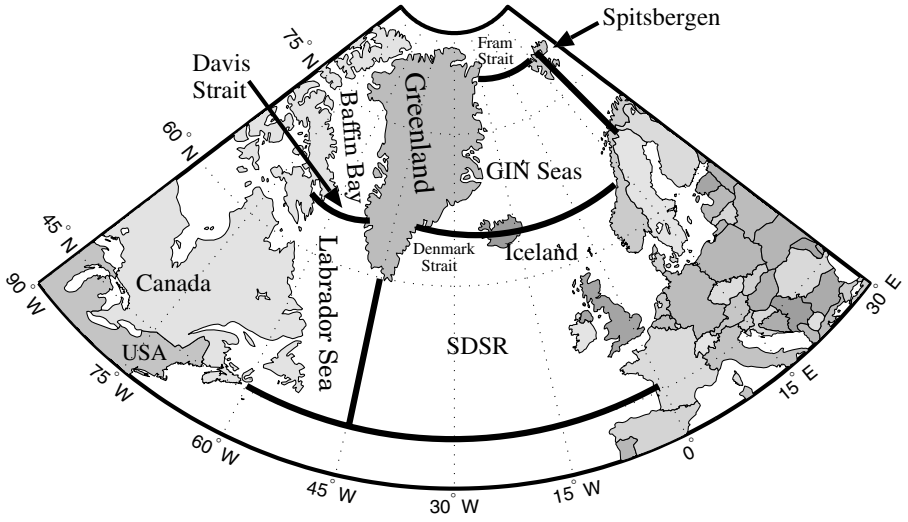

Fig. 1. A map of the North Atlantic marginal seas. The four sub-domains of interest are defined as the Labrador Sea (45°N to 65°N, west of 45°W), South of the Denmark Strait region (SDSR, 45°N to 65°N, east of 45°W), the GIN Seas (roughly 65°N to 80°N, east of 45°W to west of 20°E), and the Baffin Bay (roughly 65°N to 80°N, west of 45°W to east 80°W). In this paper, the Labrador Sea and the SDSR together are called the northern North Atlantic. The major deep ventilations for the thermohaline circulation occur in the GIN Seas, the Labrador Sea and SDSR.

ice. The atmospheric model is the National Center for Atmospheric Research (NCAR) Community Climate Model version 3 (CCM3) at T42 horizontal resolution (approximately $2.8° \times 2.8°$) with 18 hybrid levels vertically (Kiehl et al., 1998). The ocean model is a version of the Los Alamos National Laboratory Parallel Ocean Program (POP; Smith et al., 1995) with an average grid size of 2/3° (going down to 1/2° in latitude over the equatorial region) and 32 vertical levels. The land surface model is the NCAR Land Surface Model (LSM; Bonan, 1998). The sea ice model is a version of the dynamic–thermodynamic sea ice model used by Zhang and Hibler (1997) and optimized for the parallel computer environment required by the PCM. The surface climate in the PCM control simulation is stable and comparable in many ways to observations (Washington et al., 2000). In a 1000-year-long control integration, the trend of global mean surface temperature is only about 0.03 °K century-1 (Meehl et al., 2004). This coupled model has been used in a number of climate change studies (e.g., Meehl et al., 2001, 2003, 2004; Dai et al., 2001a,b; Arblaster et al., 2002; Santer et al., 2003a,b).

2.2. Experiments

A four-member ensemble of the 20th century historical simulations is analyzed here. These experiments have been documented by Meehl et al. (2003, 2004). Each of the ensemble members start from a different state of the control run about 20 years apart after the control run spins up to 1870 conditions (for details, see Washington et al., 2000). Time-evolving greenhouse gases, sulfate aerosols (direct effect only; black carbon not included), and stratospheric and tropospheric ozone are added as forcings throughout the course of the simulations from 1870 to 1999. The nature forcings (solar and volcano) have not been included in these simulations. The simulated global mean temperature from these runs varies in a similar way as the observations, especially in the last three decades of the 20th century when anthropogenic forcings were dominant compared to the natural forcings (Meehl et al., 2004), but slightly underestimates the warming in parts of the first half of the 20th century when natural forcings are more important. In the following analysis, our focus is only on climate changes in the latter part of the 20th century, and the linear trend of the control run is removed from all data.

3. Results

3.1. Simulated zonal mean changes in the North Atlantic

The simulated zonal and ensemble averaged salinity, temperature, and density changes between 1985–1999 and 1955–1969 are shown in the left panels of Fig. 2 along with the observations (right panels). The observed

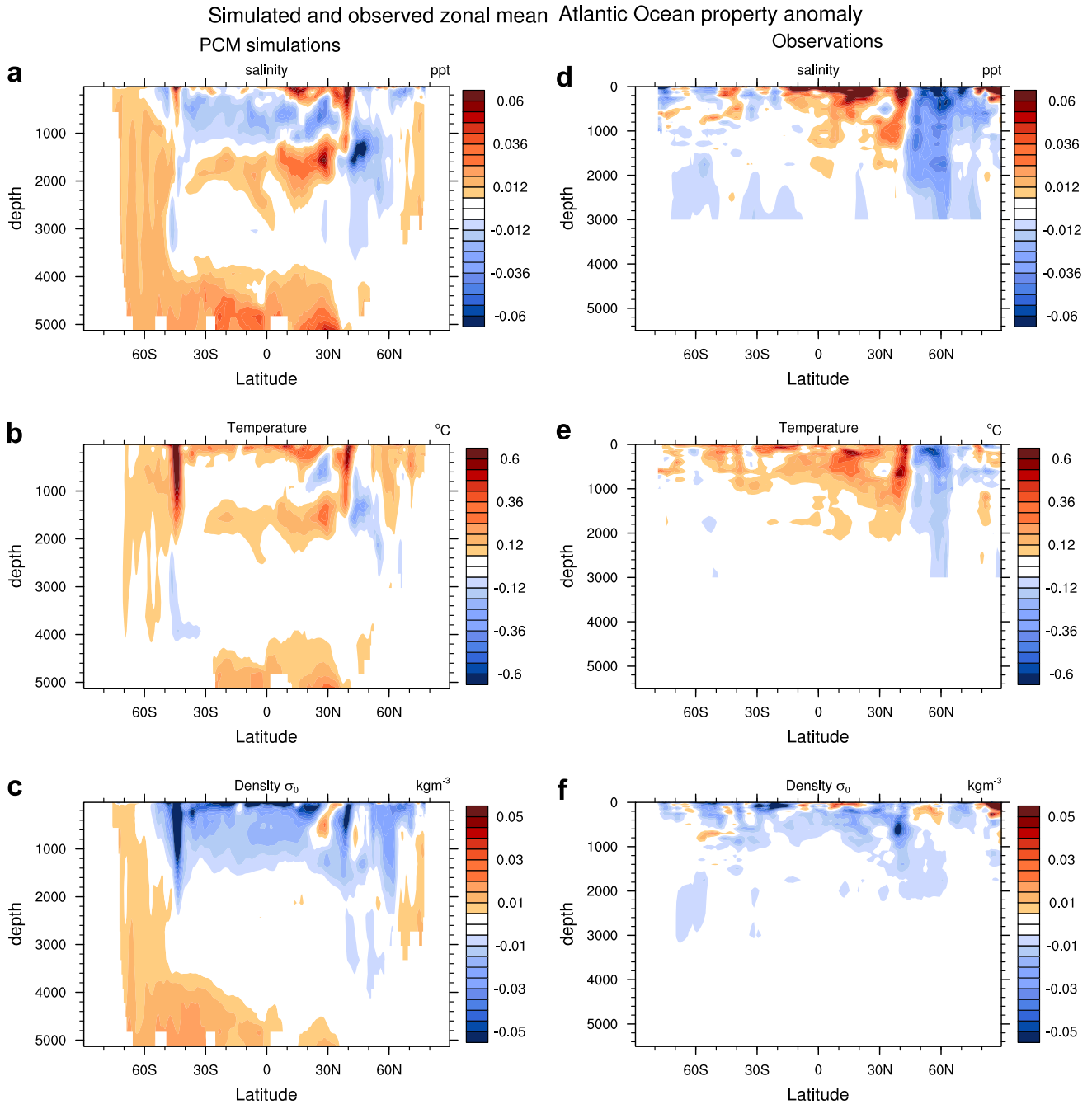

Fig. 2. Observed and simulated zonal mean changed between 1985–1999 and 1955–1969 in the Atlantic sector. Left panels are for the PCM simulations (zonal and ensemble-averaged) and right panels for observations. panels (a) and (d) are salinity anomalies, (b) and (e) are temperature anomalies, and (c) and (f) are density anomalies. The contour interval is 0.006 ppt for salinity (a, d), 0.06 °C for temperature (b, e), and 0.005 kg m^{-3} for density (c, f). Positive (negative) values indicate an increase (a decrease) in salinity, temperature or density.

data are based on the pentad anomaly of temperature (Levitus et al., 2005a), and the pentad anomaly of salinity (Boyer et al., 2005). (Note that the observation only provides the anomalies for the upper 3000 m of the ocean.) The panels of 2a and 2c are similar to the Fig. 1a and b in Hu and Meehl (2005), but with an expanded domain. The zonal mean salinity changes in our model (Fig. 2a) show similar patterns as in the observed zonal mean salinity anomalies (Fig. 2d), and are also in good agreement with Antonov et al. (2002) and Boyer et al. (2005). The simulated salinity changes are similar to the results of Curry et al. (2003) whose study is along a specific cross-section in the North Atlantic. All of these zonal mean anomalies illustrate a freshening on both sides of the subpolar Atlantic, and a more saline upper ocean in the subtropics (Fig. 2a and d). The simulated

strongest freshening in our model is in the deep North Atlantic centered at a depth of 1500 m between 42° and 50°N, agreeing with values reported by Curry et al. (2003) and Antonov et al. (2002) for the observations, but differing slightly from Fig. 2d and Boyer et al. (2005) who show a salinity change between two pentad means (1994–1998 and 1955–1959). Both Fig. 2d and Boyer et al. indicate a stronger freshening in the upper 500 m of the northern North Atlantic. On the other hand, the general agreement between simulated and observed zonal mean changes of salinity may suggest that the observed salinity changes reported by Curry et al. (2003) are not only confined to the Labrador Sea, but the entire overflow system in the northern North Atlantic may have become fresher since 1950s as reported by Dickson et al. (2002) and Antonov et al. (2002), and confirmed by Boyer et al. (2005) and Fig. 2d. In our model, a fresher sub-surface tropics and subtropics are also produced, indicating that the freshening of the Antarctic intermediate water simulated by PCM may be stronger than observed (Antonov et al., 2002; Curry et al., 2003), and also penetrate too far north than suggested by Boyer et al. (2005) and Fig. 2d. The other features, such as the freshening between 65° and 75°N, and a more saline north of 75°N, also agree with the observational study of Boyer et al. (2005) and Fig. 2d. However, the salinity increase of the Antarctic bottom water (AABW) in the model solution is not shown in the observations of Antonov et al. (2002), Curry et al. (2003), Boyer et al. (2005), or Fig. 2d.

In Fig. 2b, the zonal mean ocean temperature changes are also in good agreement with the observations (Fig. 2e; Antonov et al., 2002; Curry et al., 2003; Levitus et al., 2005a), such as a warming of the upper ocean in most parts of the Atlantic section and a cooling between 40° and 60°N in both PCM simulations and observations (Fig. 2e, also see Fig. 4b and top-right panel of Fig. 2 of Antonov et al., 2002; Fig. 2c of Curry et al., 2003; and Fig. A7 of Levitus et al., 2005a). This general agreement implies that the upper ocean temperature change is a feature for the entire zonal span of the Atlantic as shown in PCM simulation and observations of Antonov et al. (2002) and Levitus et al. (2005a). On the other hand, the cooling between 40° and 60 °N in the model is not as strong as shown in observations, and is mostly a sub-surface feature in our zonal mean data. When we looked at the sea surface temperature changes (Fig. 3b), there is a surface cooling in the eastern Labrador Sea region, which is very close to the location where the cross-section is drawn by Curry et al. (2003). But the observations (Fig. 3e) show a more uniformed cooling in most part of the Labrador Sea and SDSR. Therefore, the discrepancy between model simulated and observed cooling in the sub-surface northern North Atlantic might be possibly related to the failure of the model to reproduce the observed surface cooling associated to the upward trend of NAO in the late 20th century. On the other hand, because of the lack of volcanic forcing, the surface warming over the northern North Atlantic may have been overestimated in our model solutions in comparison to the observation.

Simulated changes of the zonal mean Atlantic density in the upper 1500 m (Fig. 2c) are almost uniform, showing a lighter upper ocean. The patterns of the simulated density changes are very close to the observed (Fig. 2f), but a bit stronger than the observed. Apparently in the tropics and subtropics, the surface warming dominates over the salinity increase to produce decreased density, and in the sub-surface, the freshening and warming both work towards a density decrease in PCM simulations. In the northern North Atlantic, the density decrease reaches more than 3000 m in model simulations, but about 2500 m in the observations. By comparing Fig. 2a and b, and Fig. 2d and f, we found the density decrease in the northern North Atlantic is mainly related to the freshening there since only the freshening can induce a density decrease and the cooling would have induced a density increase. Overall, the PCM simulations (Fig. 2c) show a lighter North Atlantic deep water (NADW) and a denser Antarctic bottom water (AABW) in 1985–1999 compared to 1955–1969, the observations mainly display a lighter NADW. The denser AABW in PCM is mainly associated with a salinity increase in the Atlantic sector of the Southern Oceans. In comparison to the observations (Antonov et al., 2005; Levitus et al., 2005b), our model results may have slightly overestimated the density decrease in the northern North Atlantic. This overestimation is related to the underestimation of the cooling in this region. Antonov et al. (2005) and Levitus et al. (2005b) show that the total steric sea level (a vertical integration of the density anomalies) for the upper 3000 m of the ocean is increased slightly in this region, owing to the compensation effect of the thermosteric changes (a cooling induced sea level decrease) and the halosteric changes (a freshening induced sea level increase). Nevertheless, this observed increase in total steric sea level indicates a decrease of the density in the whole water column (0–3000 meters) of the northern North Atlantic region.

In this paper, we focus on estimating the relative importance of the possible contributors to the subsurface freshening and cooling in the subpolar North Atlantic between 45° and 65°N (also called the Labrador Sea

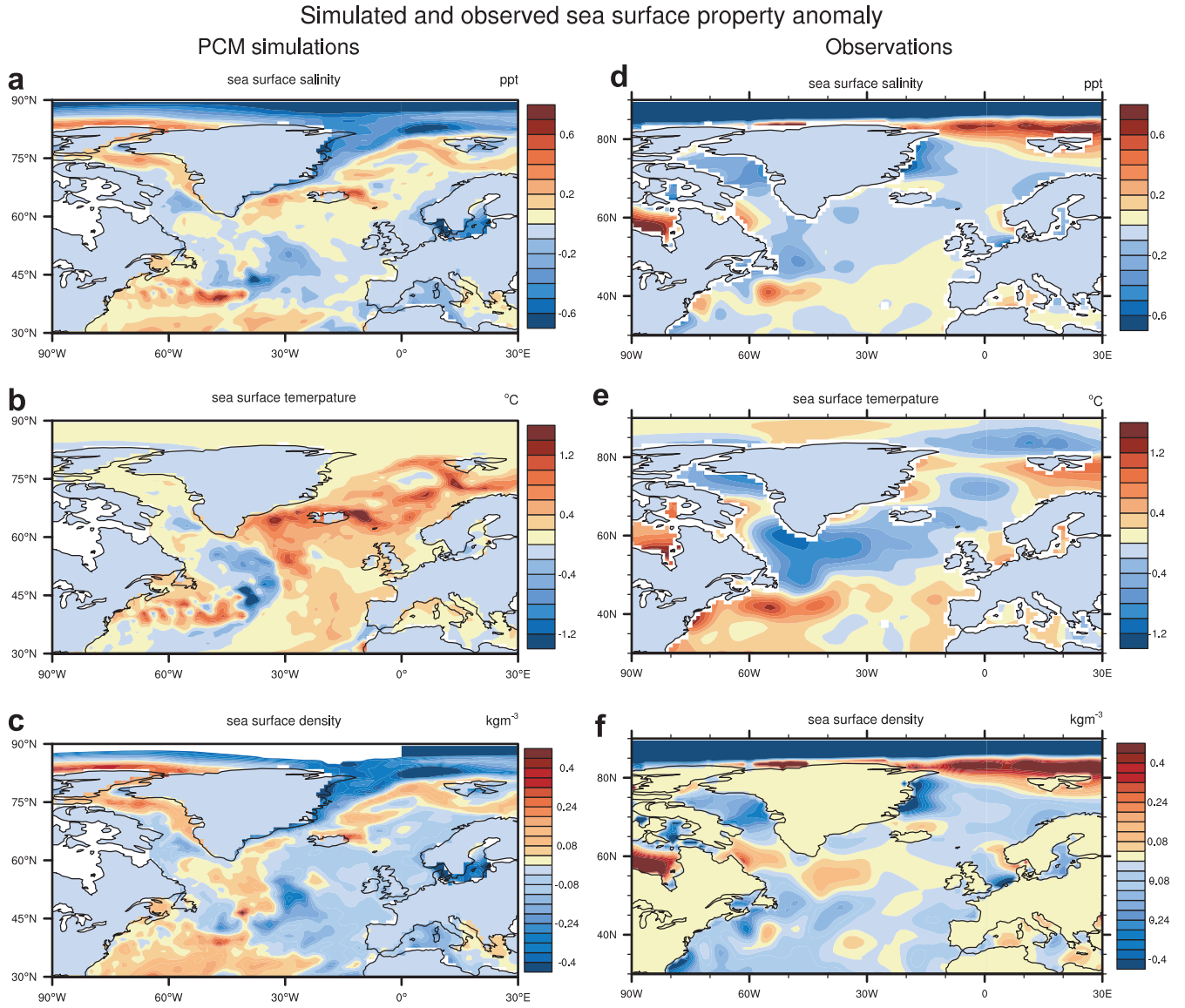

Fig. 3. Observed and simulated sea surface salinity (SSS, panels a and d), temperature (SST, panels b and e), and density (panels c and f) difference between 1985–1999 and 1955–1969 in the North Atlantic. Left panels are for the PCM simulations and right panels for observations. The contour interval is 0.2 °C for temperature, 0.1 ppt for salinity, and 0.04 kg m^{-3} for density. Positive (negative) values represent an increase (a decrease) in surface temperature, salinity, or density.

and south of the Denmark Strait region, or the northern North Atlantic in this paper) through a freshwater and heat budget analysis.

3.2. Variations of the surface properties in North Atlantic

Before analyzing the changes in surface forcings, such as P–E, sea ice flux, and surface heat flux, we first look at the variations of the sea surface temperature (SST), salinity (SSS) and density which are directly influenced by the surface fluxes. The dominant pattern of sea surface salinity change is a salinity increase in most parts of the northern North Atlantic in the PCM (Fig. 3a), but a salinity decrease in the observations (Fig. 3d). This discrepancy may be associated to the underestimation of the precipitation changes in PCM which will be discussed in more detail in Section 3.3. At south of 45°N, the simulated and observed salinity changes are in better agreement, both showing an increase in SSS related to increased evaporation there. The simulated SSS changes are also in good agreement with observed east of the Greenland coast region, possibly related to the increased ice melting there.

The dominant pattern of the simulated SST change is warming, especially in the eastern part of the northern North Atlantic and in the GIN Seas with an amplitude up to 1 °C. The surface cooling is confined west of 30°W, between 35° and 50°N (Fig. 3a). In the observations (Fig. 3e), the warming shows up south of the 45°N, and the eastern and western coast regions of the GIN Seas. The cooling occupies most parts of the northern North Atlantic and the central GIN Seas. Thus the PCM simulations failed to reproduce the observed SST changes in most parts of the northern North Atlantic, except the eastern Labrador Sea region. This may be related to the failure of PCM to reproduce the observed upward NAO-trend in the second half of the 20th century.

The simulated surface density changes show that most parts of the surface North Atlantic become lighter, indicating that the warming dominates the surface density change (Fig. 3c). These changes are similar to the observation (Fig. 3f). However, the observed surface density changes are more related to the surface freshening. In some parts of the Labrador Sea, the surface density is increased owing to the surface cooling and salinity increase in both observations and the PCM simulations. The density increase to the north of Iceland and south of Spitsbergen is due to the shrinking of the sea ice cover, leading to a decrease in local sea ice melting and a higher salinity in both Fig. 3c and f.

3.3. Observed and simulated North Atlantic oscillation (NAO)

The North Atlantic Oscillation (NAO) is the dominant mode of atmospheric variability in the North Atlantic region and represents a redistribution of atmospheric mass between centers of action located near the Azores high and the Icelandic low. During the high NAO phase, both the Azores high and the Icelandic low are strengthened, resulting in an increased sea level pressure (SLP) gradient between these two centers, and leading to a stronger westerly flow. This has been associated to changes in surface air temperature (SAT) and precipitation in the North Atlantic region (Hurrell, 1995; 1996; Dai et al., 1997; Marshall et al., 2001). The Arctic Oscillation is the dominant mode of variability in the Northern Hemisphere and displays an annular pattern related to a decreased SLP over the Arctic basin and an increased SLP at midlatitudes with two centers of action in the North Atlantic and North Pacific. Studies show that the Arctic Oscillation (or the northern annular mode) is closely correlated to the NAO, with a correlation coefficient of 0.95 for the observed monthly time series (e.g., Deser, 2000). Since our major concern is the northern North Atlantic, we use NAO to represent the atmospheric variability in this region.

The NAO index used here is based on the Empirical Orthogonal Function analysis (EOF) to optimal representation of the spatial pattern associated with NAO. Following Hurrell (1995), we use the time series of the leading EOF of the seasonal mean (December to March) SLP anomalies between 20° and 80°N, and 90°W to 40°E as the NAO index, as shown in Fig. 4. Three NAO time series are shown in this figure which are from the European Centre for Medium-Range Weather Forecasting (ECMWF) 40-year reanalysis data (ERA-40) (upper), Trenberth and Paolino (1980) Northern Hemisphere SLP data (middle), and PCM ensemble (lower). The NAO index from ERA-40 data and Trenberth and Paolino data are almost the same for the overlapping period with a correlation of 0.99. The simulated NAO index from PCM does not exhibit an upward trend since 1970 as shown in the observed NAO index, and does not correlate with the observed NAO index either. The cause of the observed upward NAO trend in the late 20th century is still an ongoing research topic. The reason for the failure to reproduce the observed NAO trend in the PCM simulations is unclear and under investigation, but is out of the scope of this paper.

The correlation patterns of the NAO index with the Northern Hemisphere SLP are shown in Fig. 5. The observed patterns (the left and middle panels in Fig. 5) show the NAO index is positively correlated with the Azores High and negatively to the Icelandic Low, and with very weak correlation with the Pacific SLP. The correlation patterns in the PCM ensemble are similar to the observed patterns in the Atlantic sector which is important to our study, but the difference is large in the Pacific side which shows that the changes in Pacific SLP are strongly correlated with that in the Atlantic.

3.4. Changes in surface heat and freshwater fluxes

The surface freshwater flux includes the P–E and sea ice flux. Fig. 6 is a comparison of the climatological precipitation pattern in the model simulation (PCM), the ERA-40 reanalysis data, and observations (land

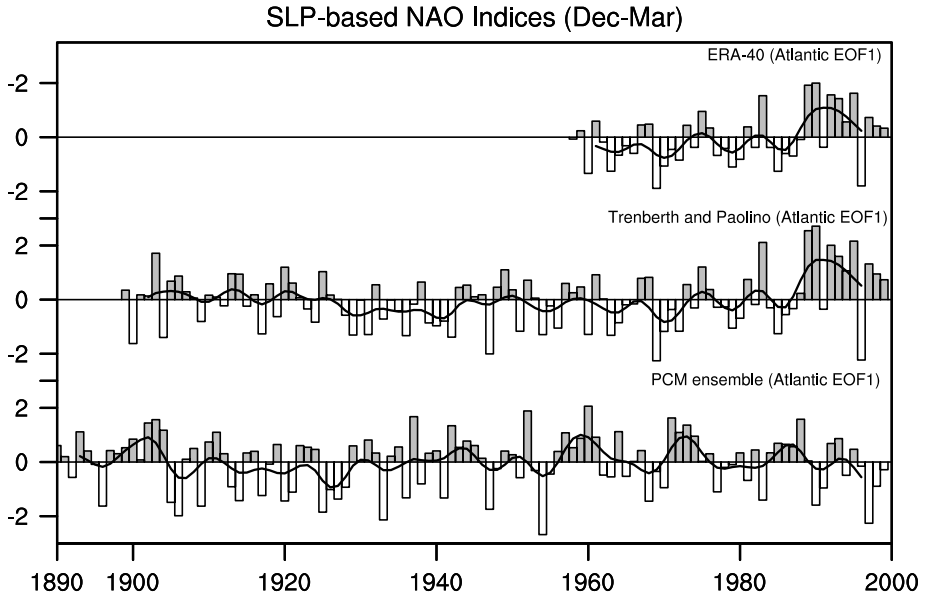

Fig. 4. Observed and modeled North Atlantic Oscillation (NAO) index time series based on the first EOF of the winter season (December to March) Atlantic sea level pressure (SLP) anomalies (20–80°N, 80°W–40°E). The upper panel is for the ERA-40 data, middle panel for Trenberth and Paolino SLP data, and the bottom panel for PCM ensemble.

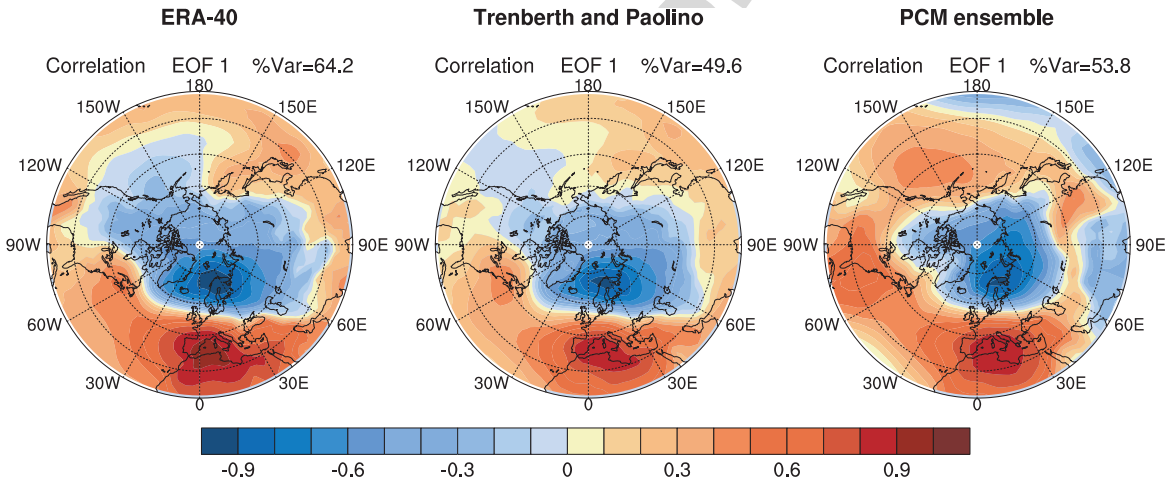

Fig. 5. Correlation patterns of the observed and modeled North Atlantic Oscillation (NAO) index with the Northern Hemisphere sea level pressure (SLP). Left panel is for the ERA-40 data, middle panel for Trenberth and Paolino SLP data, and the right panel for PCM ensemble. Contour interval is 0.1.

only, Xie and Arkin, 1996; Dai et al., 1997; Mitchell et al., 2004). The observed precipitation patterns on both sides of the Atlantic are similar between the high resolution CRUTS data (Fig. 6b) and the low resolution blended Dai et al. and Xie and Arkin data (Fig. 6a), with greater precipitation amounts in land areas that border the North Atlantic. The reanalysis data (Fig. 6c) and PCM simulations (Fig. 6d) show qualitative agreement with the observed data over land areas. They both capture the major precipitation patterns on land, such as a higher precipitation at the southern tip of Greenland, and the coastal regions of Scandinavia. On the other hand, the reanalysis data underestimates the precipitation in the eastern United States, and the simulated precipitation in PCM agrees better with the observations than the ERA-40 data in this region. If it is assumed that the reanalysis precipitation over the North Atlantic ocean is correct, the PCM overestimates the precipitation over the eastern part of the ocean.

The observed precipitation anomalies over land show patterns related to the positive phase of NAO, with increased precipitation from northeast America to Iceland and northern Europe, and decreased precipitation

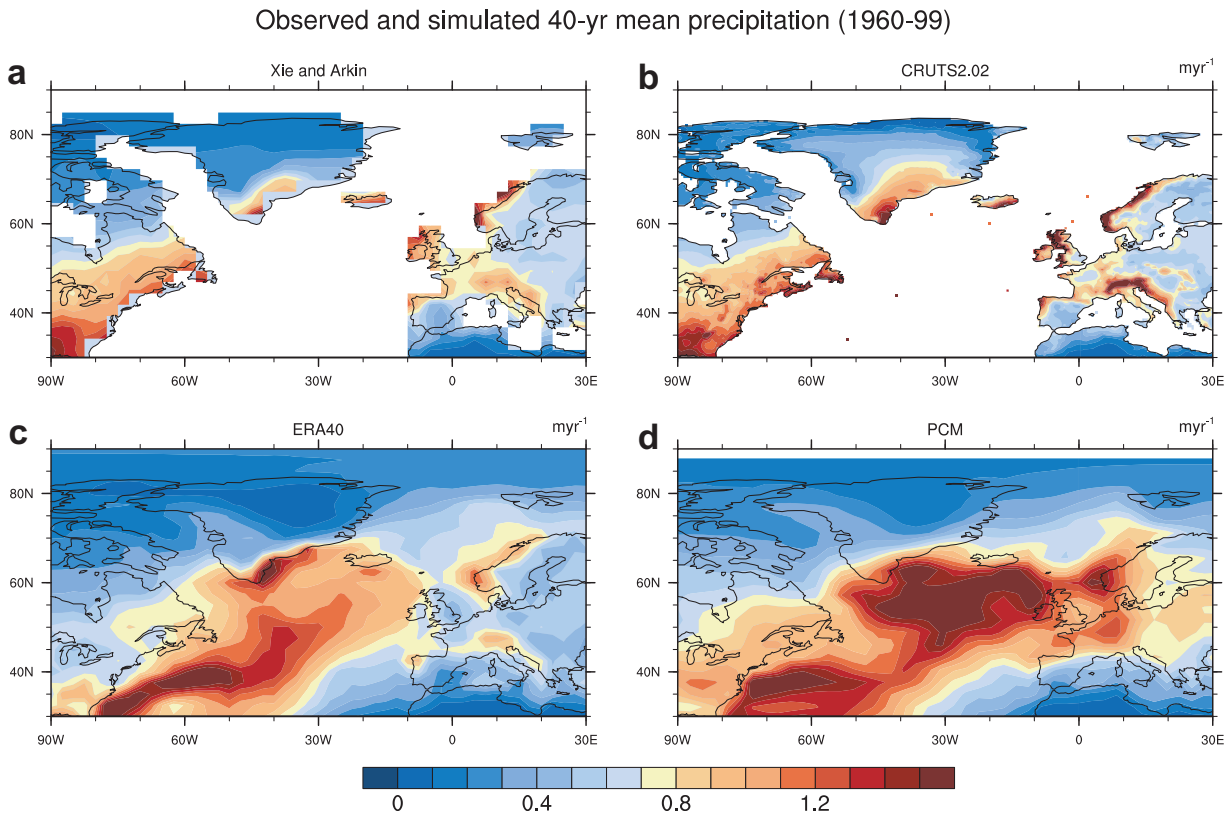

Fig. 6. Observed and simulated climatological precipitation in the North Atlantic: 1. Observations: Xie and Arkin (a), CRUTS2.02 (b); 2. Reanalyzed: ERA-40 (c); and 3. Simulated by PCM (d). Contour interval is 0.1 myr^{-1}.

along the Canada and the southern Greenland coasts, and mid-south Europe in the period 1985–1999 compared to 1955–1969 (Fig. 7a and b). By assuming that the precipitation anomaly pattern over the northern North Atlantic ocean is related to that over North America and Europe, we see that the ERA-40 data possibly overestimates the increase of precipitation in the northern North Atlantic ocean region since the ERA-40 data shows an increase in precipitation almost everywhere in the North Atlantic (Fig. 7c). On the other hand, simulated precipitation changes by PCM are different in some ways to the observations, with the model producing increases in precipitation over the North Atlantic near Iceland as suggested by the observations, but decreases over the northeast U.S. stretching across the Atlantic near 50°N. Previous studies show that the precipitation changes in the North Atlantic region are largely related to variations of NAO (e.g., Hurrell, 1995; Dai et al., 1997; Marshall et al., 2001). There is a significant upward trend in the observed NAO during the second half of the 20th century. This NAO trend is absent from our model simulation, which may be the reason for the discrepancy between PCM simulations and observations. The overall precipitation over the northern North Atlantic slightly decreases in our model, instead of a large increase as in ERA-40 data.

The precipitation only represents a one-way water exchange from air to sea. Water also evaporates from sea to air. To consider the net surface freshwater input into the ocean, both precipitation and evaporation need to be taken into account. The net change of surface freshwater flux due to P–E is shown in Fig. 8 (positive values indicate an increase in P–E). In the reanalysis data (Fig. 8a), P–E increases almost everywhere in the northern North Atlantic. The largest increase is located in the northeastern North Atlantic between Iceland and England, related to increased precipitation and decreased evaporation. In PCM simulations (Fig. 8b), the P–E changes show a mixed pattern with increases west of 35°W and regions south of Iceland, and a decrease in most parts of the mid-eastern North Atlantic. Given that the precipitation changes in ERA-40 are likely to be overestimated, the estimation of the regional mean P–E changes in PCM may not be too different from reality.

The geographic distribution of the simulated changes in net surface heat and freshwater fluxes is shown in Fig. 9 (positive values indicate an increased oceanic heat loss or freshwater gain). The net surface freshwater

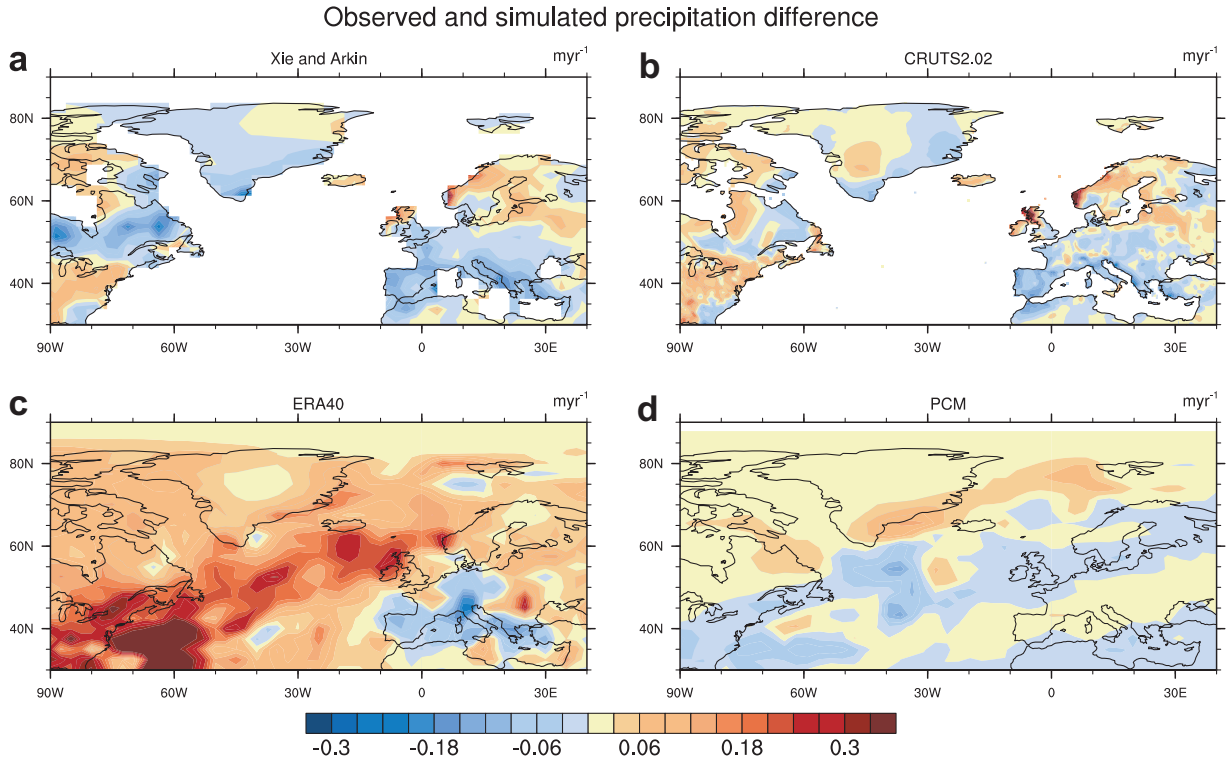

Fig. 7. Observed and simulated changes of precipitation between 1985–1999 and 1955–1969. Contour interval is 0.03 myr^{-1}. Positive (negative) values indicate a precipitation increase (decrease) in period 1985–1999 relative to period 1955–1969.

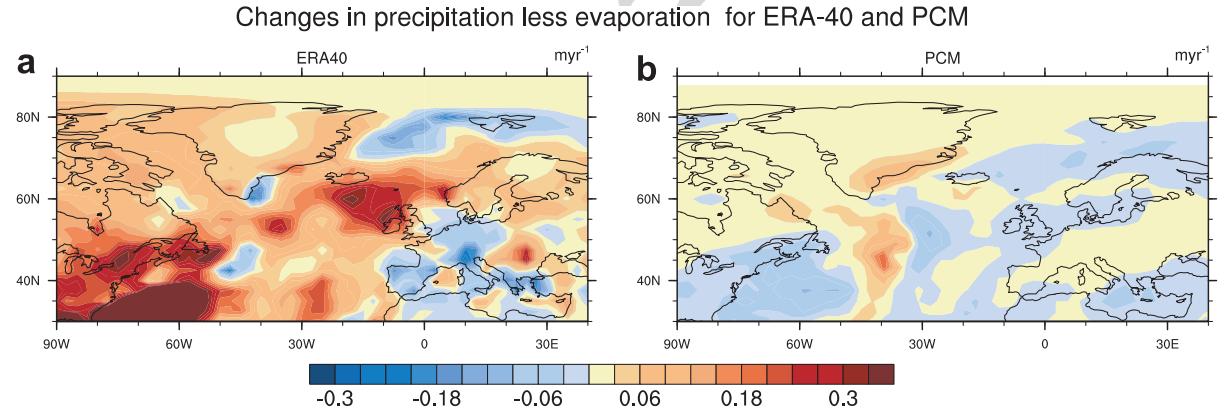

Fig. 8. Changes of the precipitation less evaporation between 1985–1999 and 1955–1969 from ERA-40 (a) and PCM (b). Positive values indicate an increase in P–E. Contour interval is 0.03 myr^{-1}. Positive (negative) values represent an increase (a decrease) in the precipitation less evaporation in the later period relative to the earlier period.

fluxes include the P–E, sea ice flux, and local ice melting. Here the sea ice flux is defined as the ice transported from other regions (mostly from the Arctic via the GIN Seas) into the northern North Atlantic, and the local sea ice melting is defined as the net melting of the ice existing locally. In other words, the result of this local ice melting is a net loss of the local ice volume. In Fig. 9a, the pattern of the net surface freshwater flux change differs from the P–E changes in Fig. 8b. In Fig. 9a, positive differences indicate an increase of surface freshwater input. The most significant changes in Fig. 9a are south of the Denmark Strait, off the coast of Greenland. These changes are related to the decrease of sea ice cover, thus producing a decrease in local sea ice melting. In the Labrador Sea, the decreased surface fresh water flux is also caused by decreased local sea ice melting associated with a reduction in sea ice flux exported from the Arctic to this region (see next subsection for more details). In most of the SDSR (see Fig. 1 for its definition), the net surface freshwater input changes agree with the P–E changes in Fig. 8b, owing to less sea ice related effect.

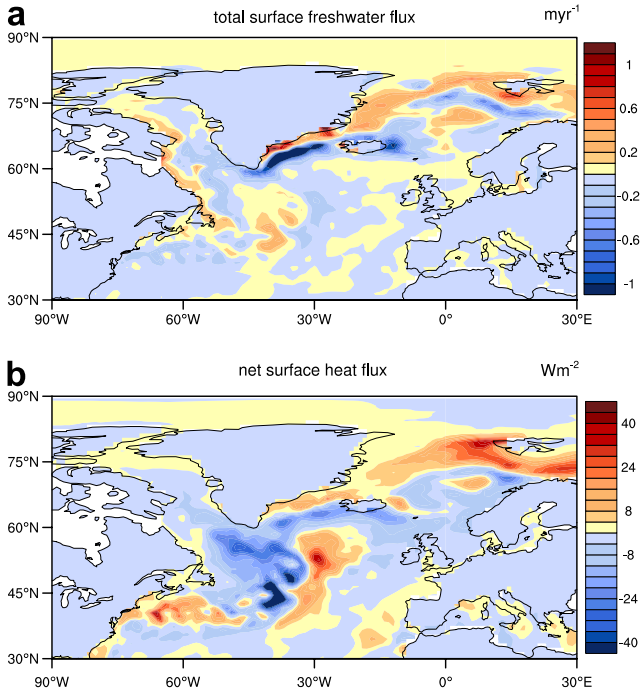

Fig. 9. Changes of the net surface heat and freshwater fluxes between 1985–1999 and 1955–1969. Note: the net surface freshwater flux includes both P–E and sea ice. The sign convention is that positive values indicate an increased oceanic heat loss or freshwater gain.

In general, there is a net heat loss from the ocean to the atmosphere north of 40°N. Fig. 9a shows decreased heat loss in the Labrador Sea and the eastern and western parts of the SDSR (positive regions). In comparison with Fig. 3a, most of the areas with decreased heat loss are related to warmer SSTs, except the western part of the SDSR which is associated with a cooler sea surface temperature. In the warmer sea surface temperature regions, the CO_2 induced warming heats up the air above the ocean, reducing the air–sea temperature contrast, leading to a reduced oceanic heat loss. The increase of the net heat loss (negative differences) in the middle of the SDSR and the decrease in the western part of the SDSR are associated with an eastward movement of the North Atlantic current pathway in the PCM simulations. This eastward movement of the North Atlantic current pathway is related to a weaker THC in the PCM simulation (Dai et al., 2005). Since the North Atlantic current is an extension of the Gulf Stream, this current carries a significant amount of heat to the northern North Atlantic and GIN Seas. Thus the shift in this current's pathway affects the intensity of the local air–sea interaction, and the sea surface temperature as shown in Figs. 9a and 3.

The time evolution of the P–E and net surface heat flux in the Labrador Sea and the SDSR is shown in Fig. 10. Since the 1950s, P–E shows an increasing trend of 0.00048 Sv/decade in the Labrador Sea, and a decreasing trend of 0.00002 Sv/decade in the SDSR (Fig. 10d and f). The total change of P–E in these two regions is a 0.0014 Sv increase from 1955–1969 to 1985–1999 as shown in Hu and Meehl (2005), thus contributing to the zonal mean salinity decrease in this region. In Fig. 10c and e, the heat loss in both regions is reduced since the 1950s, with a trend of -2.35 Wm^{-2}/decade for the Labrador Sea and -1.77 Wm^{-2}/decade for the SDSR. This reduction in net surface oceanic heat loss is consistent with the surface warming, and is a result of warmer local air temperature preventing a high heat loss from the ocean, but negatively related to the sub-surface cooling between 40° and 60°N as shown in Fig. 2b.

3.5. Changes in sea ice flux

In general, there is net freshwater input into the Arctic Ocean due to precipitation and river runoff. In order to balance this freshwater gain, the Arctic exports sea ice and fresher ocean water into the GIN Seas and further south into the North Atlantic and the other parts of the global ocean. Variations in this fresh-

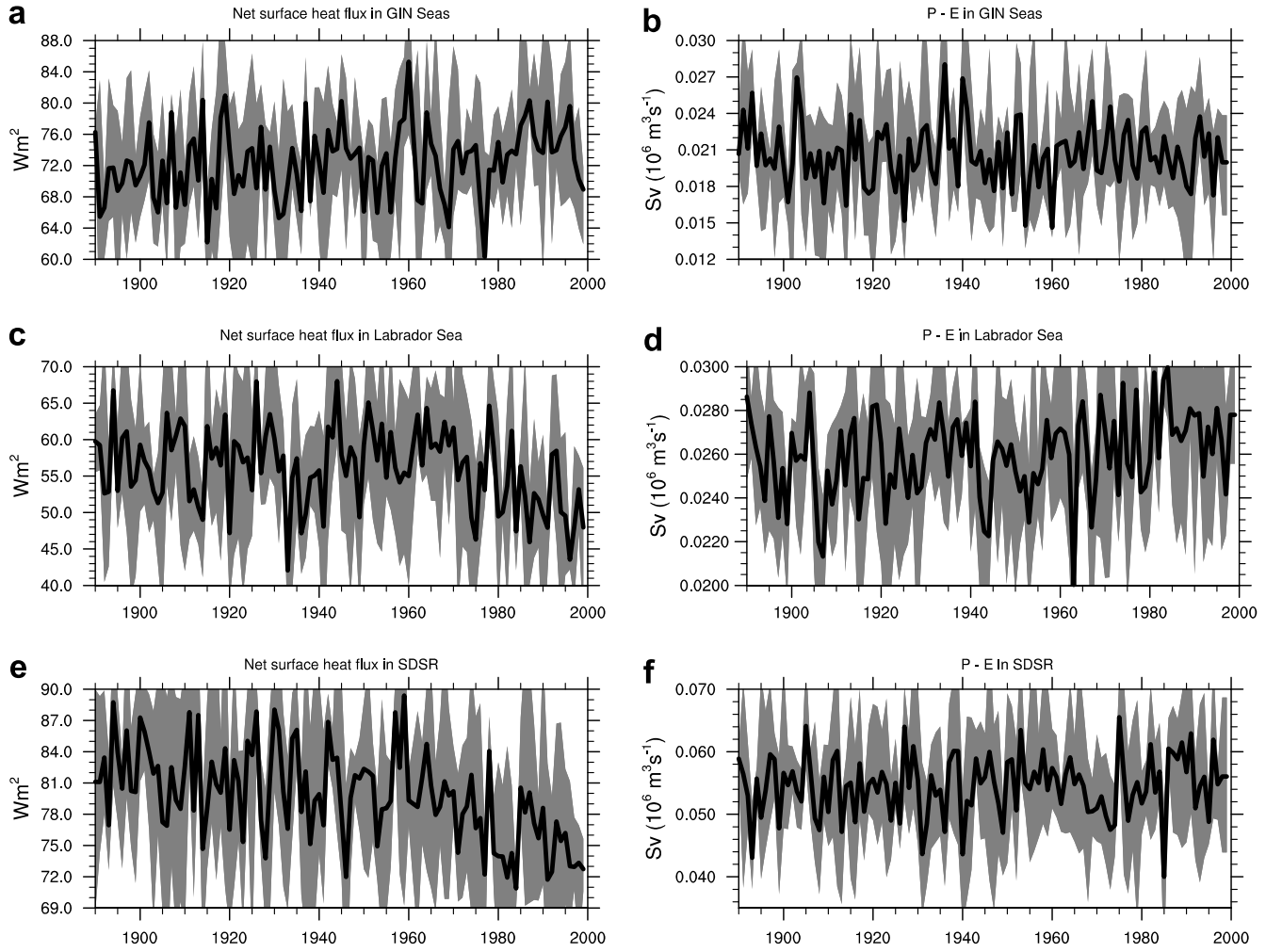

Fig. 10. Time evolution of the net surface heat flux and P–E in GIN Seas (panels a and b), Labrador Sea (panels c and d), south of the Denmark Strait region (e and f). The shading in this figure and others indicate the ensemble range.

water export will affect the oceanic stratification in the GIN Seas and the northern North Atlantic and the freshwater budget in the Arctic. As shown in Fig. 11, the exported sea ice fluxes from the Arctic to the GIN Seas through both the Fram Strait and Barents Sea reduces by 10.7% and 23.5% from 1950s to 1990s, respectively. The sea ice fluxes from the GIN Seas via the Denmark Strait and from Baffin Bay via the Davis Strait into the northern North Atlantic (between 45° and 65°N) reduce by 17.4% and 1%, respectively. As a result, the total sea ice flux convergence in the northern North Atlantic reduces by 15.6% from 1955–1969 to 1985–1999. On the other hand, the annual mean sea ice volume in the northern North Atlantic is decreased by 31.1 km^3, roughly 7% (Fig. 12b). This decrease of local sea ice volume means an increase in freshwater supply to this region due to ice melting, or a decrease of the local freshwater reserve, thus it partly compensates for the reduced sea ice flux into this region. The overall reduction of the freshwater flux due to sea ice in this region is about 10%, from 0.1055 Sv in 1955–1969 to 0.0940 Sv in 1985–1999, with a negative trend of 0.0038 Sv/decade since 1950. Thus, the total surface freshwater input, P–E plus sea ice flux, shows a decrease, with a net reduction of about 0.0101 Sv, or 5% as reported in Hu and Meehl (2005).

On the other hand, the reduction in sea ice flux from the Arctic into the Labrador Sea and SDSR implies that less heat is used to melt that ice locally, contributing positively to the surface warming in those regions. And the reduction in sea ice volume and also in sea ice extent (not shown) in the Labrador Sea induces a lower surface albedo. This leads to an enhanced absorption of solar radiation by the ocean. Thus the net effect of these sea ice changes on ocean surface temperature is to warm up the ocean.

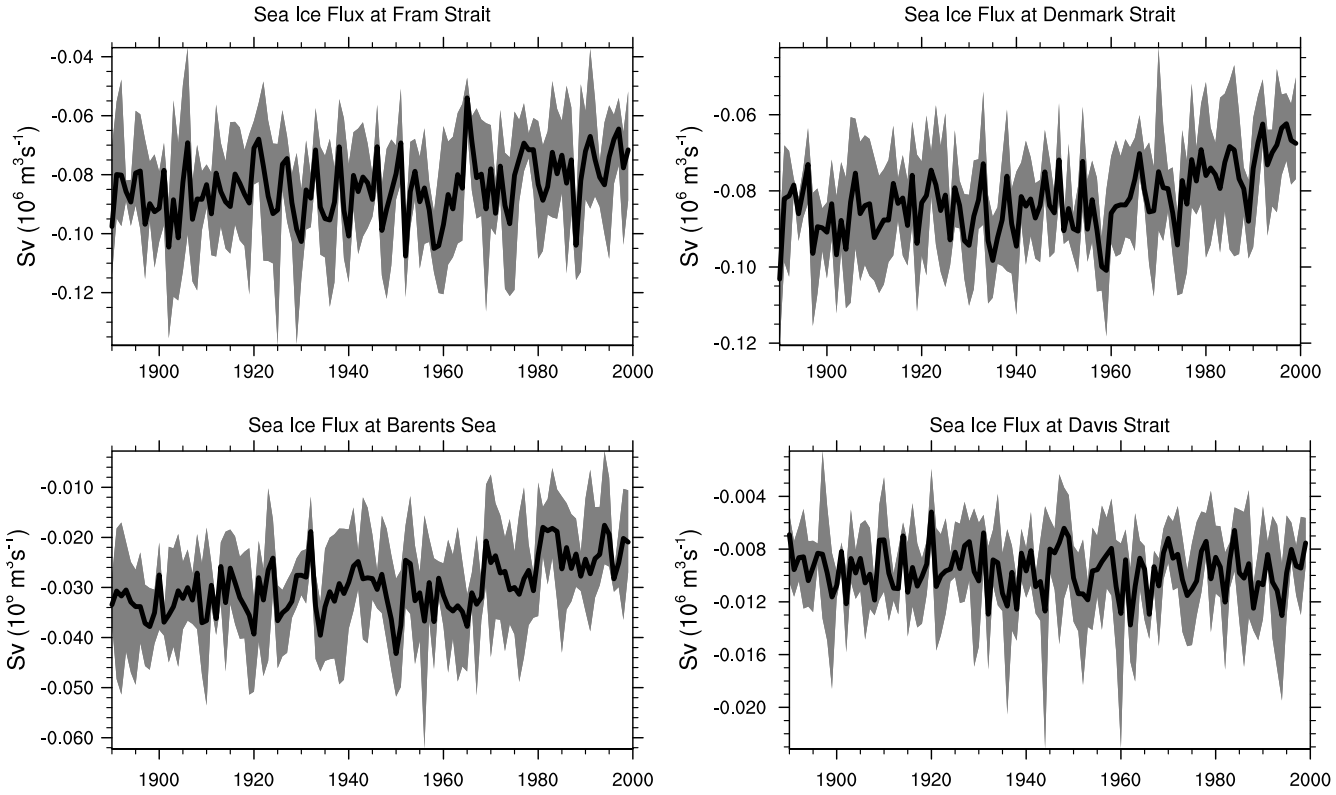

Fig. 11. Time evolution of the sea ice fluxes at the Fram Strait (a), the Denmark Strait (b), the Davis Strait (d), and from the Barents Sea to GIN Seas (c).

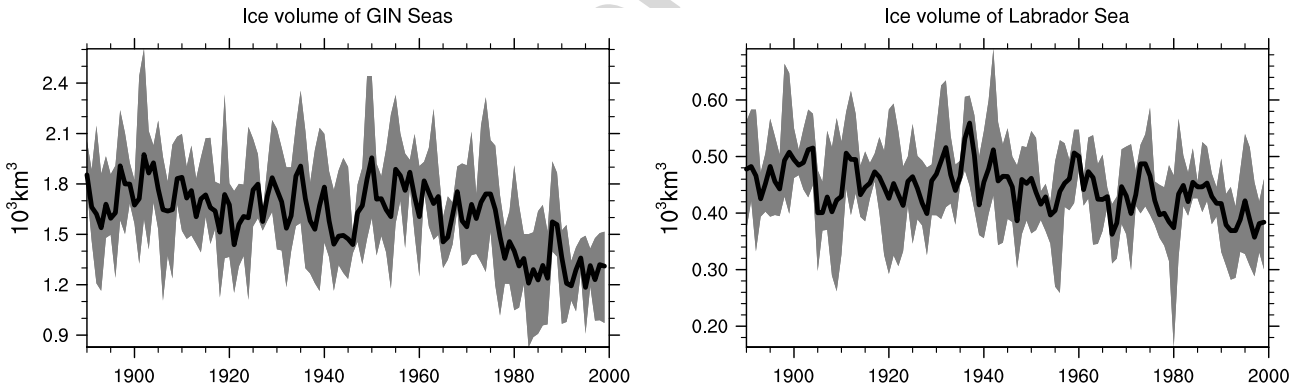

Fig. 12. Variations of the sea ice volume in the GIN Seas (a) and in the Labrador Sea (b) from 1890 to 1999.

3.6. Changes in meridional heat and freshwater transports

In the Atlantic, the meridional heat transport is mainly carried by the THC. Since the deep ventilation only happens in the subpolar North Atlantic and around the periphery of the Antarctic, there is a net northward meridional heat transport in the Atlantic resulting from an import of warmer upper water and an export of the colder North Atlantic Deep Water (NADW) to other parts of the world oceans. The northward meridional heat transport decreases at 45°N with a linear trend of 0.0135 PW/decade (1 PW a $\equiv 10^{15}$ W), and increases at 65°N with a trend of 0.0031 PW/decade since the 1950s in the ensemble averaged model simulation (Fig. 13a and c). The increased meridional heat transport at 65°N contributes positively to the simulated warming in the GIN Seas which induces an increased heat loss from the ocean to the atmosphere as shown in Fig. 10a. On the other hand, the resulting meridional heat divergence between 45° and 65°N increases

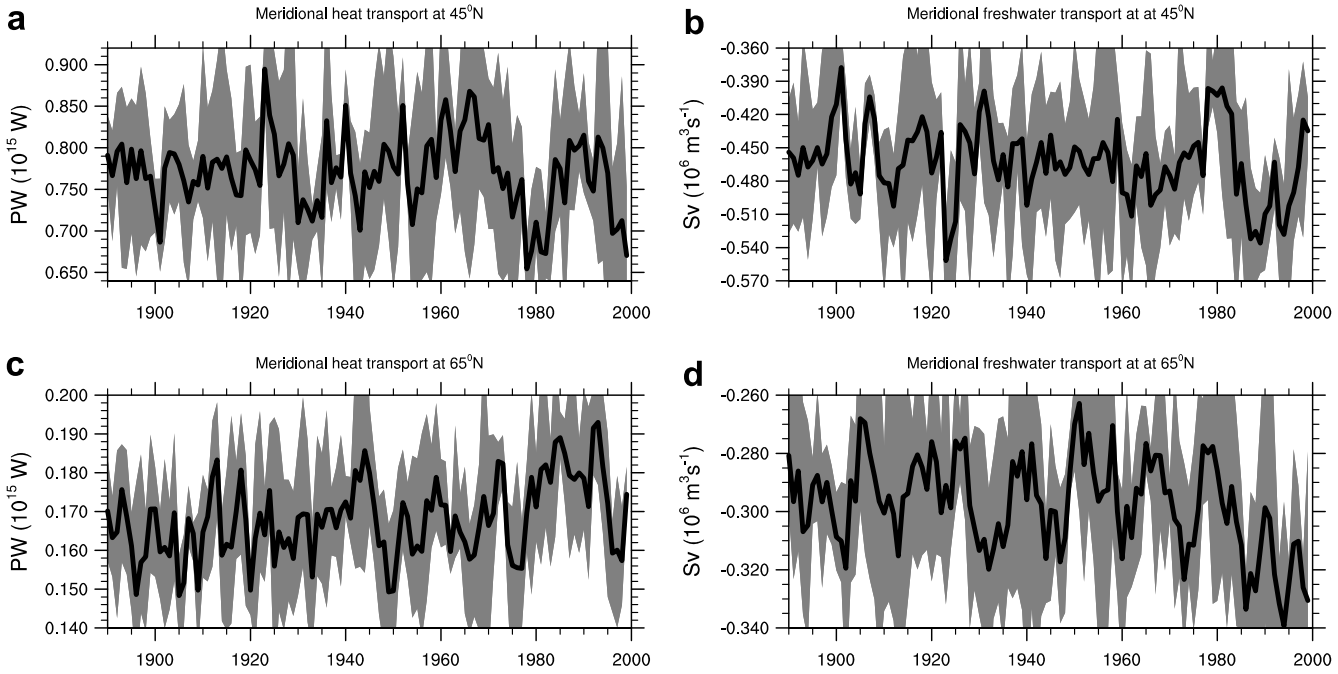

Fig. 13. Time evolution of the oceanic meridional heat transport at 45°N (a) and 65°N (c), and the oceanic meridional freshwater transport at 45°N (b) and 65°N (d). The positive (negative) values indicate a northward (southward) transport of heat (freshwater).

by 0.0777 PW from 1955–1969 to 1985–1999. This increase in meridional heat divergence leads to a net heat loss in this region, thus causing a sub-surface cooling effect.

The THC not only transports heat meridionally, but it also transports freshwater. In contrast to a net northward meridional heat transport, the meridional freshwater transport in the Atlantic is southward (e.g., Wijffels et al., 1992; Dababasoglu and McWillianms, 1995; Rahmstorf, 1996; Lohmann, 2003). The southward meridional freshwater transport at 45°N changes from 0.4737 Sv in 1955–1969 period to 0.4935 Sv in 1985–1999 period, with a linear trend of +0.0037 Sv/decade (Fig. 13b). At 65°N, this southward freshwater transport increases from 0.2920 Sv in the earlier period to 0.3223 Sv in the later period with a trend of +0.0088 Sv/decade (Fig. 13d). Because the increase of freshwater transport at 65°N is higher than at 45°N, the meridional freshwater divergence between these two latitudes decreases, resulting in a freshwater gain of about 0.0105 Sv in this region (Hu and Meehl, 2005). This decrease of freshwater divergence is related to a weakening of the THC which will be discussed later. Subtracting the freshwater deficit at the surface, there is a 0.0004 Sv net freshwater gain in this region. In other words, the fresher North Atlantic between 45° and 65°N is mainly due to the decreased meridional freshwater divergence (or increased freshwater convergence) in our model which is related to a weaker THC as discussed later.

The increased southward meridional freshwater transport at 65°N is related to the global warming induced P–E and sea ice changes in the Arctic and GIN Seas. The P–E changes in these regions are small in our simulations, with an increase of about 1% from 1955–1969 to 1985–1999. On the other hand, the warming induces much more significant changes in the Arctic sea ice cover. Both of the sea ice extent and thickness in the Arctic decrease with a linear trend of 0.214 million km^2/decade and 2.9 cm/decade, respectively, since 1950 (Fig. 14). The total Arctic sea ice extent shrinks from 15.46 million km^2 in 1955–1969 to 14.86 million km^2 in 1985–1999, and the mean sea ice thickness reduces from 1.959 m to 1.853 m. These changes qualitatively agree with observations which show a loss of Arctic sea ice extent and thickness (e.g., Walsh and Johnson, 1979; Maslanik et al., 1996; Parkinson et al., 1999; Rothrock et al., 1999; Vinnikov et al., 1999).

The sea ice volume (a combination of the sea ice extent and thickness) in the Arctic reduces by 3300 km^3 or about 11% from 29.3×10^3 km^3 in the period 1955–1969 to 26.0×10^3 km^3 in the period 1985–1999, with a trend of 0.94×10^3 km^3/decade in the PCM simulations. The total freshwater input in the Arctic increases by about 50% due to this loss of sea ice volume. The Arctic sea surface salinity is lowered by this increased freshwater input, with a mean decrease about 0.16 psu (Fig. 3b).

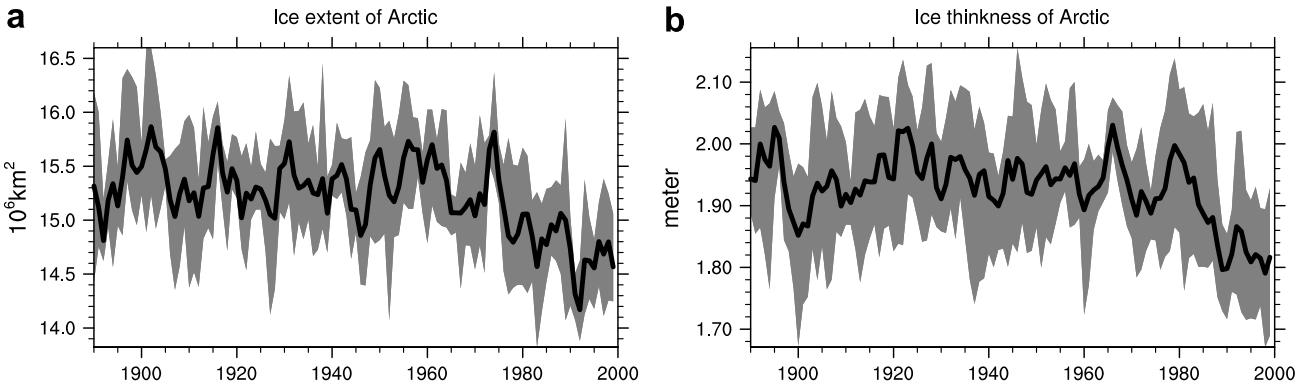

Fig. 14. The Arctic sea ice extent (a) and thickness (b).

In the GIN Seas, the sea ice flux convergence decreases from 0.033 Sv to 0.030 Sv from 1955–1965 to 1985–1999. The sea ice volume changes from 1704 to 1312 km^3 between the same two periods, about 398 km^3 or a 23% reduction (Fig. 12a). Taking into account the increased P–E as shown in Fig. 10b, the total supply of the freshwater flux increases by about 0.0098 Sv from 1955–1965 to 1985-1999 in this region. Therefore, when the freshwater anomaly in the Arctic and GIN Seas exits at Denmark Strait and Feroa Bank, the southward freshwater transport increases there.

3.7. Changes in the thermohaline circulation

Both meridional heat and freshwater transports are related to the strength of the THC. The meridional overturning streamfunction averaged over 1955–1969 is shown in Fig. 15a. The maximum strength is about 31.6 Sv, which is stronger than values suggested by observational studies – about 14–20 Sv (e.g., Hall and Bryden, 1982; Roemmich and Wunsch, 1985; McCartney and Talley, 1984). The mean meridional overturning in 1985–1999 weakens compared to 1955–1969 (Fig. 15b). The weakening is up to 2.5 Sv centered at 35°N and about 2500 m deep. In comparison to the meridional streamfunction in Fig. 15a, the maximum changes of the meridional overturning do not overlap with the meridional streamfunction maximum, but lie about 1000 m below it. This indicates a retreat in the maximum penetration depth of the deep convection in the North Atlantic. As a result, the whole meridional overturning cell associated with the North Atlantic deep water moves upward, or becomes shallower.

Fig. 15b also shows that in the upper North Atlantic, the meridional overturning actually strengthens north of 40°N, indicating an enhanced northward transport of the upper warmer water in the 1985–1999 period than in the 1955–1965 period (Note that changes occur in upper 1 km). On the other hand, the northward transport of the warmer, salty subtropical water is reduced since the meridional overturning in the upper ocean is weakened south of 40°N. These changes in meridional overturning induce a decreased northward meridional heat transport from the tropical and subtropical Atlantic to the Labrador Sea and the SDSR, and an increased meridional heat transport from the Labrador Sea and the SDSR to the GIN Seas. As a result, the meridional heat divergence increases in the Labrador Sea and the SDSR, leading to a mid-depth cooling.

To better relate the changes in THC with the changes of meridional heat and freshwater transports, the THC index is calculated using the maximum strength of the meridional streamfunction in the Atlantic (see Fig. 1e in Hu and Meehl, 2005). The THC weakens by about 1.2 Sv in the second period relative to the first, with a decreasing trend of 0.33 Sv/decade since 1950. Associated with the THC, the northward heat transport in the North Atlantic is quasi-linearly correlated with the strength of THC (e.g., Bryan and Holland, 1989; Smith et al., 2000; Hu, 2001). A weaker THC, in general, transports less heat into the North Atlantic, as shown in Fig. 13a. The correlation between THC and meridional heat transport at 45°N is 0.85 for the second half of the 20th century. On the other hand, the CO_2 induced warming effect induces a non-uniform change of the deep convection in the Labrador Sea, the SDSR, and the GIN Seas as reported by Hu et al. (2004a). As a result, the northward meridional heat transport north of roughly 55°N increases as THC weakens (Fig. 13c). Therefore, the meridional heat transport at 65°N is negatively correlated to the THC in the PCM simulations.

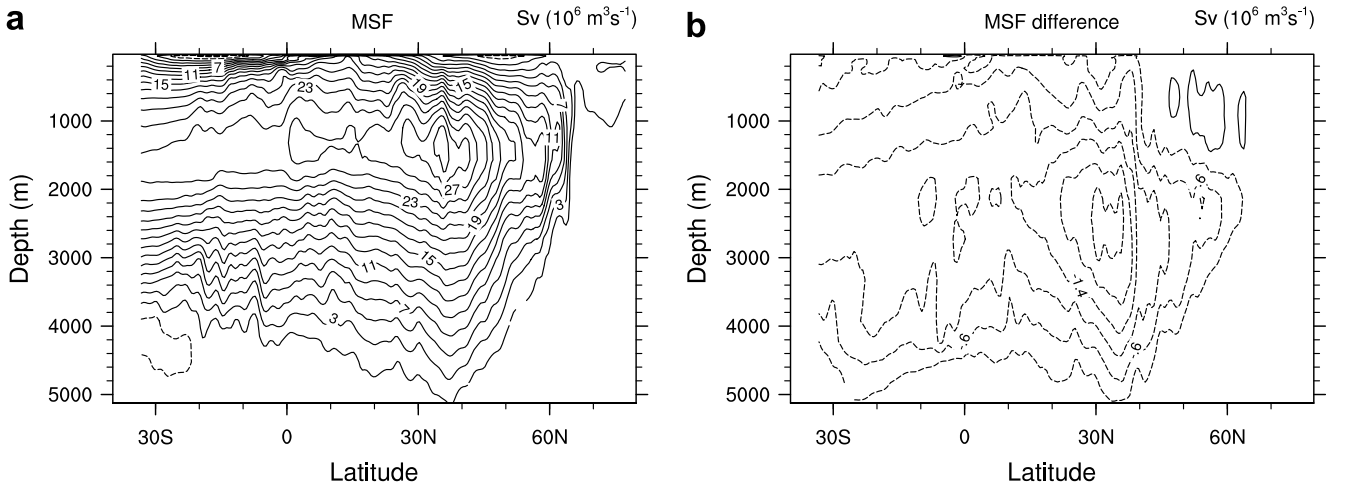

Fig. 15. The mean meridional streamfunction (MSF) in the Atlantic (a) and changes of MSF between 1985–1999 and 1955–1969. The contour interval is 2 Sv for panel (a) and 0.4 Sv for panel (b).

The meridional freshwater transport is positively correlated to the THC at 45°N, negatively at 65°N. In other words, a weaker THC transports less freshwater southward at 45°N, and more at 65°N, leading to a decreased meridional freshwater divergence and a fresher ocean between 45° and 65°N, further weakening the THC, and vice versa for a stronger THC. The lag correlation shows that the THC leads the meridional freshwater divergence in the northern North Atlantic by one year, with a lag −1 correlation coefficient of 0.66 for the last 50 years of the 20th century. Thus, associated with the greenhouse gas induced global warming effect, as the THC becomes weaker, the ability of the THC to transport the freshwater anomaly from the northern North Atlantic is reduced.

The scatter plots in Fig. 16 illustrate the relation of the THC strength and the meridional freshwater divergence (Fig. 16a), and the relationship of the THC and the meridional heat convergence (Fig. 16b) between 45° and 65°N since 1950 in the PCM simulations. It is very clear from Fig. 16 that a stronger THC is related to a stronger meridional freshwater divergence, and to a stronger meridional heat convergence in the northern North Atlantic. As THC becomes weaker in our simulation, both the meridional freshwater divergence and the meridional heat convergence are decreased, inducing a freshening and cooling effect in this region.

3.8. Causes of the slower THC

The strength of THC can be affected by many factors, such as surface freshwater and heat flux anomalies in the North Atlantic marginal seas, changes of winds, inter-basin salinity or temperature contrast, or remote

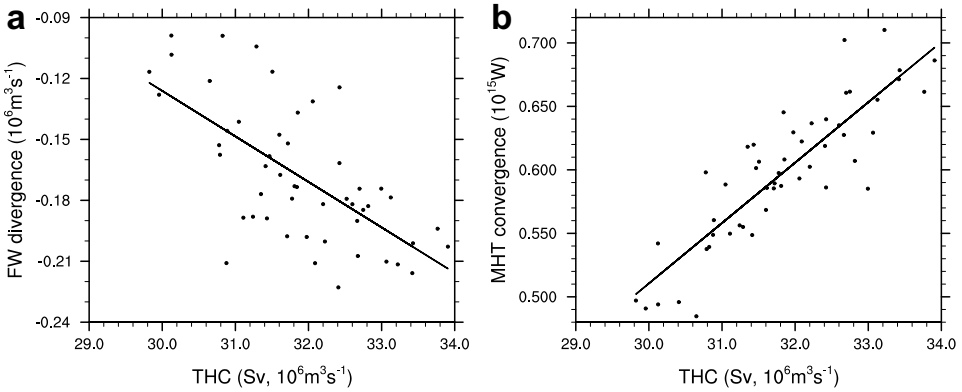

Fig. 16. Scatter plot: (a) the THC index with the meridional freshwater divergence between 45° and 65°N; (b) the THC index with the meridional heat convergence between the same latitude band as in panel (a).

effects in tropical regions or southern ocean (e.g., Gent, 2001; Hu et al., 2004b; Seidov and Haupt, 2003, 2005; Toggweiler and Samuels, 1998; Ruhlemann et al., 1999). Here we first examine the inter-basin sea surface salinity and temperature contrasts between North Atlantic and North Pacific, then examine the local direct effects of the heat and freshwater flux changes in the North Atlantic and the Arctic.

As shown by Stott et al. (2000), Meehl et al. (2003, 2004) and Broccoli et al. (2003), the warming in the late 20th century is mainly induced by the increase of atmospheric CO_2 concentrations. This global warming is the ultimate reason for a weaker THC in PCM simulations in the late 20th century. The global warming intensifies the hydrological cycle, such as increased precipitation in the polar and sub-polar region, and an increased evaporation in the subtropics (e.g., Dai et al., 2001a; Hu et al., 2004a). On the other hand, this warming also causes changes in the cryosphere, such as a retreat of glaciers (not included in PCM) and reduced sea ice cover. These processes will change the sea surface density and ocean vertical stratification, and thus affect the strength of the THC.

Seidov and Haupt (2003, 2005) demonstrated that the inter-basin sea surface salinity contrast between the North Atlantic and North Pacific (10–60°N) controls the strength of the THC in equilibrium state. How this inter-basin salinity contrast will affect the THC under transient forcing is not very clear. By using the NCAR community climate system model version 2 (CCSM2), Hu et al. (2004b) show that this sea surface salinity contrast is a good indicator of the THC changes under century time-scale transient forcings if the freshwater anomaly is the primary cause for the THC variability. If the thermal effect is the dominate cause of the THC changes, the inter-basin salinity contrast usually acts against the thermal induced THC changes. In our simulations, the inter-basin salinity contrast increases by about 0.057 psu from 1955–1969 to 1985–1999. This increase is related to a more intensified evaporation in subtropical North Atlantic and an increased precipitation in North Pacific. Thus, the inter-basin sea surface salinity contrast between North Atlantic and North Pacific intends to strengthen the THC. On the other hand, as shown later, the density changes associated with the CO_2 induced warming in the northern North Atlantic dominate this increased inter-basin salinity contrast, producing a weaker THC in our simulations.

On the other hand, Hu et al. (2004b) proposed that the sea surface temperature contrast between the North Atlantic and the North Pacific may also be used as an indicator of THC changes, with a higher contrast associated to a weaker THC. The inter-basin temperature contrast increases by 0.025 °C from 1955–1959 to 1985–1999, related to a higher warming (0.240 °C) in the North Pacific and a lower warming (0.215 °C) in the North Atlantic. This result from PCM is consistent with Hu et al. (2004b). As explained by Hu et al. (2004b), a weaker THC, in general, draws less heat from the other parts of the world ocean into the North Atlantic. Thus the North Atlantic tends to become colder, and the North Pacific tends to become a bit warmer, vice versa for a stronger THC. Under CO_2 induced warming effect, the surface warming in the North Pacific tends to be stronger than in North Atlantic. There are two primary reasons: (1) a warmer North Pacific suppresses the upwelling process, thus keep more heat at surface ocean; (2) a warmer North Atlantic tends to suppress the deep convection there, thus weakens the THC. At the same time, part of the surface heat is still deposited into the deeper ocean through deep ventilation, and a weaker THC transports less heat meridionally to the North Atlantic. They both tend to weaken the CO_2 induced warming in the North Atlantic, thus increase the sea surface temperature contrast between the North Atlantic and the North Pacific.

Locally, the surface density decrease in most parts of the SDSR is a result dominated by the surface warming induced mainly by increased atmospheric CO_2 concentration (Fig. 3c). This decrease in surface density enhances the upper ocean vertical stratification in the SDSR, leading to weaker deep convective activity. In the eastern Labrador Sea and western SDSR, the surface density increase is associated with the cooling induced by the eastward shift of the North Atlantic current pathway and the salinity increase is related to a reduced sea ice flux from the Arctic to the Labrador Sea. This increase in the surface density may have enhanced the deep convection in those regions. The total deep ventilation in the Labrador Sea and the SDSR at a depth of 1400 m where the maximum of the meridional streamfunction is located (Fig. 13a), reduces by 0.7 Sv from 1955–1969 to 1985–1999. In the GIN Seas, the deep convection strengthens at north of the Iceland, mid-GIN Seas and south of Spitsbergen, and weakens along the Greenland coastal region and in the Norwegian Sea. The strengthening of the deep convection in the GIN Seas is associated with the reduced sea ice cover, and the weakening is related to the increased melt-ice water exported from the Arctic in the Greenland costal region, and to the warming in the Norwegian Sea. Overall, the deep convection in the

GIN Seas at 1400-m depth strengthens by about 0.15 Sv. Therefore, the total deep convection in the Labrador Sea, the SDSR, and the GIN Seas is decreased, thus producing a weaker THC in the late 20th century.

4. Conclusion and discussion

In this paper, we discuss the possible reasons for the observed freshening and cooling of the subpolar North Atlantic using a global coupled model, the Parallel Climate Model (PCM). The simulated patterns of the freshening and cooling in the subpolar North Atlantic between 45° and 65°N in late 20th century is similar to those suggested by observational studies (e.g., Antonov et al., 2002; Curry et al., 2003; Levitus et al., 2005a; Boyer et al., 2005). The changes of P–E between 1955–1965 and 1985–1999 indicate an increase in freshwater input in this region, but the reduced sea ice fluxes from the Arctic and Baffin Bay into this region change the P–E induced freshwater surplus to a deficit. Thus, the total surface freshwater flux, P–E and sea ice flux (including both imported sea ice and reduction of local sea ice), is in favor of a saltier surface ocean as shown in Fig. 3b. On the other hand, the meridional freshwater divergence in this region is reduced in the late 20th century, inducing a freshwater gain. This freshwater gain not only compensates the deficit of the surface freshwater input, but also leads to a net freshwater gain in this region, which is responsible for the simulated freshening. The changes of the net surface heat flux in the northern North Atlantic are in favor of a warmer upper ocean since the net heat loss is decreased in the late 20th century. As shown in Fig. 3a, the sea surface temperature increases in most parts of the northern North Atlantic, as opposed to the sub-surface cooling in Fig. 2b. But the meridional heat divergence is increased, with a decreased northward meridional heat transport at 45°N and an increased northward heat transport at 65°N, leading to a net heat loss in this region and contributing to the sub-surface cooling.

The changes of the meridional freshwater and heat divergence are caused by a weaker THC in our simulations. And the weakening of the THC is primarily related to the CO_2 induced global warming in the late 20th century. This global warming intensifies the global hydrological cycle, such as increased precipitation in the polar and sub-polar regions, and increased evaporation in the subtropics. The global warming also changes the cryosphere, such as a decrease in Arctic sea ice cover. In the Labrador Sea and south Denmark Strait region (see Fig. 1 for their definition), the weakening of the deep convection is mainly associated with a warmer sea surface temperature, which reduces the surface density and stabilizes the upper ocean stratification. In the GIN Seas, the deep convection is slightly intensified owing to the reduced sea ice cover there, which causes an increased sea surface salinity north of Iceland, south of Spitsbergen, and mid-GIN Seas (Fig. 3c), thus weakening the upper ocean stratification in those regions, and inducing stronger deep convection. The total deep convection in the Labrador Sea, south of the Denmark Strait region, and the GIN Seas is weakened in the late 20th century, producing a weaker THC.

This result differs from a recent model study by Wu et al. (2004) using HadCM3 who successfully simulated the observed freshening of the northeast Atlantic deep water (NEADW) since the 1950s as shown in Fig. 1a of Dickson et al. (2002) with a stronger THC. They concluded that the observed freshening may not be an indicator of the THC weakening in the late 20th century. From their Fig. 3a, it is clear that the THC strengthening is related to a salinity increase in the upper ocean of the northern North Atlantic and the GIN Seas. This salinity increase induces a higher upper ocean density in those regions in the 1980s in comparison to the 1950s (their Fig. 3b), enhancing the deep convective activity there, producing a stronger THC in their model. In this model, one of the major biases is the sea ice cover which affects the deep convection in the northern North Atlantic. The simulated sea ice coverage is greater than observed, especially in the GIN Seas. Although the observed estimates suggest that only about 20% of the sea ice exported to the GIN Seas from Arctic exits the Denmark Strait into the Labrador Sea (e.g., Aagard and Carmack, 1989), in our model simulations, roughly 70% of that sea ice flux is exported into the Labrador Sea and south of the Denmark Strait region. Therefore, the variability of the sea ice flux in the northern North Atlantic between 45° and 65°N is possibly overestimated in our simulations in comparison to reality.

On the other hand, the simulated changes of P–E in the northern North Atlantic are likely underestimated (at least relative to the ERA-40 reanalysis data). This underestimation is possibly related to the failure of this coupled model in simulating the upward trend of the NAO shown in the observations in the last 50 years of the 20th century. Studies have related the changes of the P–E in the northern North Atlantic to the variations of

the NAO (e.g., Hurrell, 1995; Dai et al., 1997; Marshall et al., 2001). Overall, our model simulations may have underestimated the changes of P–E, but overestimated the changes of sea ice fluxes in the northern North Atlantic region. In reality, the total surface freshwater input in this region, including both P–E and sea ice flux, may have increased, such as in the ERA-40 reanalysis data. This increased surface freshwater supply, combined with the greenhouse gas induced warming, would have contributed to a much more stable vertical stratification, thus producing weaker deep convection in the northern North Atlantic, and a weaker THC.

Satellite and in situ observations show a decrease in both the sea ice covered area and thickness in the Arctic, possibly due to global warming (e.g., Parkinson, 2000; Rothrock et al., 1999). Our model simulation agrees with those observations. The melt-ice water is exported from the Arctic to GIN Seas and the northern North Atlantic through wind-driven and thermohaline-driven circulations, thus inducing a positive freshwater anomaly along melt-ice water pathway. This freshwater anomaly, plus the greenhouse gas induced surface warming, stabilizes the upper ocean by decreasing the upper ocean density, suppresses deep convection, and contributes to a weaker THC.

Thus, the relative importance of the surface warming and each of the freshwater sources for the possible slower THC in the late 20th century in northern North Atlantic may be different in reality and in our model, but the ocean's decreased ability to transport the freshwater anomaly out of the northern North Atlantic and the increased poleward meridional heat transport north of 55°N caused by a CO_2 induced weaker THC are likely to be major contributors to the freshening and cooling in this region both in observations and in our model.

In this study, we emphasized that the changes of the THC is the major contributor of the simulated freshening and cooling in the northern North Atlantic. Previous studies (e.g., Delworth and Dixon, 2000; Hu, 2001; Eden and Jung, 2001) show that variations of THC are related to the NAO variability. By artificially adding an upward trend of the NAO since 1970s in a coupled model, Delworth and Dixon (2000) found that this upward trend of NAO in the late 20th century may have strengthened the THC. Using an ocean model driven by the surface flux patterns of heat, freshwater, and momentum associated with the NAO, Eden and Jung found that the THC lags the inter-decadal NAO variability about 10 to 20 years with a relation of a stronger THC corresponding to a higher NAO. In a coupled ice-ocean model forced by idealized NAO variability derived from NCAR/NCEP reanalysis data, Hu (2001) found that in a quasi-equilibrium state, the THC is stronger in high NAO phase than in low NAO phase. If this ice-ocean model is forced by an idealized NAO variation with combined lower (70 years) and higher (10 years) frequencies, the THC tends to become weaker during the first half of the integration when the NAO index is lower, and to be stronger during the second half when the NAO index is higher, but with a much smaller amplitude in comparison with the quasi-equilibrium experiments. Hu concluded that a persistent high (low) NAO phase is needed to significantly affect the strength of THC, and an inter-annually varying NAO might not be able to produce a significant trend in THC. Hu (2001) also indicates that the stronger THC during high NAO phase is mainly related to the strengthened deep convection in the Labrador Sea due to increased sea surface salinity. Nevertheless, all of these studies indicate a possible strengthening of the THC during a persistent high NAO phase.

Since the upward trend of the NAO is missing in the PCM simulation, does this mean that PCM simulations are biased towards a weaker THC, or the fact of the PCM simulations being able to resemble the observed changes in the northern North Atlantic is due to model biases? The answer is very likely to be no. A recent observational study of the meridional transport at 25°N in the Atlantic shows a stable Gulf Stream transport at the Florida Strait with an increased wind-driven return flow in the subtropical interior ocean and a decreased southward flow of deep water since 1950s (Bryden et al., 2005). Bryden et al. (2005) concluded that the THC may have weakened by up to 30% along a decreased meridional heat transport. Considering the overall decrease in sea surface density in the northern North Atlantic dominated by freshening effect which might imply a more stable oceanic stratification in this region, thus possibly a weakened deep convection (see Figs. 2 and 3), Bryden et al.'s study is in concert with these observations in sub-polar North Atlantic. Although there are some uncertainties in the study of Bryden et al. (2005) and uncertainties in the subpolar observations, such as reported by Dickson et al. (2002), Curry et al. (2003), Antonov et al. (2002, 2005), Levitus et al. (2005a), Boyer et al. (2005), the evidence of oceanic property changes in the subpolar North Atlantic seems to imply a weaker deep convection, thus a weaker THC in the late 20th century. As shown by Hu (2001), a stronger THC in high NAO phase is resulting from a more saline Labrador Sea which is in contra-

diction with the observations. On the other hand, the NAO might not be the only factor which can influence the THC or the deep convection in the subpolar North Atlantic marginal seas. Other factors may also affect the changes of THC, e.g. the meridional gradient of the zonally averaged steric height (Hughes and Weaver, 1994; Thorpe et al., 2001), inter-basin salinity contrast (Stocker et al., 1992; Seidov and Haupt, 2003, 2005), the southern ocean freshening (Saenko et al., 2003), and the warming of tropical Atlantic upper ocean (Ruhlemann et al., 1999), inter-basin SST contrast (Hu et al., 2004b). Therefore the simulated weakening of THC in the late 20th century in PCM is very likely to be true in reality.

Acknowledgements

The authors thank the constructive and insight comments from Ronald Stouffer and an anonymous reviewer which improved our manuscript significantly. We thank Drs. Kevin Trenberth and Aiguo Dai for comments on the comparison of observed and ERA-40 precipitation data sets, Dr. Marika Holland for her comments on changes of the GIN Sea deep convection, and Dr. Ruth Curry for her kindness to provide us her observed data and updated plots. We thank Stephanie Shearer for help in text editing. A portion of this study was supported by the Office of Biological and Environmental Research, U.S. Department of Energy, as part of its Climate Change Prediction Program. The National Center for Atmospheric Research is sponsored by the National Science Foundation (NSF). Weiqing han is supported by NSF grant OCE-0136836.

References

Aagard, K., Carmack, E.C., 1989. The role of sea ice and other fresh water in the Arctic circulation. J. Geophys. Res. 94, 14485–14498.

Abdalati, W., Steffen, K., 1997. Snowmelt on the Greenland ice sheet as derived from passive microwave satellite data. J. Clim. 10, 165–175.

Antonov, J.I., Levitus, S., Boyer, T.P., 2002. Steric sea level variations during 1957–1994: Importance of salinity. J. Geophys. Res. 107, 8013. doi:10.1029/2001JC000964.

Antonov, J.I., Levitus, S., Boyer, T.P., 2005. Thermosteric sea level rise, 1955–2003. Geophys. Res. Lett. 32, L12602. doi:10.1029/2005GL023112.

Arblaster, J.M., Meehl, G.A., Moore, A.M., 2002. Interdecadal modulation of Australian rainfall. Clim. Dyn. 18, 519–531.

Belkin, I.M., Levitus, S., Antonov, J.I., Malmberg, S.-A., 1998. Great salinity anomalies in the North Atlantic. Prog. Oceanogr. 41, 1–68.

Bonan, G.B., 1998. The land surface climatology of the NCAR Land Surface Model coupled to the NCAR Community Climate Model. J. Climate 11, 1307–1326.

Boyer, T.P., Levitus, S., Antonov, J.I., Locarnini, R.A., Garcia, H.E., 2005. Linear trends in salinity for the world ocean, 1955–1998. Geophys. Res. Lett. 32, L01604. doi:10.1029/2004GL021791.

Broccoli, A.J., Dixon, K.W., Delworth, T.L., Knutson, T.R., Stouffer, R.J., Zeng, F., 2003. Twentieth-century temperature and precipitation trends in ensemble climate simulations including natural and anthropogenic forcing. J. Geophys. Res. 108, 4798. doi:10.1029/2003JD003812.

Bryan, F.O., and Holland, W.R., 1989. A high resolution simulation of the wind- and thermohaline-driven circulation in the North Atlantic Ocean. In: Mller, P. and Henderson, D. (Eds.), Parameterization of Small Scale Processes: Proceedings of the Aha Huliko'a Hawaiian Winter Workshop. Spec. Publ. 99-116 Hawaii Inst. of Geophys. Honolulu.

Bryden, H.L., Longworth, H.R., Cunningham, S.A., 2005. Slowing of the Atlantic meridional overturning circulation at 25°N. Nature 438, 655–657.

Cubasch, U. et al., 2001. Projections of future climate change. In: Houghton, J.T. et al. (Eds.), Climate Change 2001: The Scientific Basis-Contribution of Working Group I to the Third Assessment Report of the Intergovernment Panel on Climate Change. Cambridge Univ. Press, New York, pp. 525–582.

Curry, R., Dickson, B., Yashayaev, I., 2003. A change in the freshwater balance of the Atlantic Ocean over the past four decades. Nature 426, 826–829.

Dababasoglu, G., McWillianms, J.C., 1995. Sensitivity of the global ocean circulation to parameterizations of mesoscale tracer transports. J. Clim. 8, 2967–2987.

Dai, A., Fung, I.Y., Del Genio, A.D., 1997. Surface observed global land precipitation variations during 1900–88. J. Clim. 10, 2943–2962.

Dai, A., Wigley, T.M.L., Boville, B.A., Kiehl, J.T., Buja, L.E., 2001a. Climates of the twentieth and twenty-first centuries simulated by the NCAR climate system model. J. Climate 14, 485–519.

Dai, A., Wigley, T.M.L., Meehl, G.A., Washington, W.M., 2001b. Effects of stabilizing atmospheric CO_2 on global climate in the next two centuries. Geophys. Res. Lett. 28, 4511–4514.

Dai, A., Hu, A., Meehl, G.A., Washington, W.M., Strand, W.G., 2005. Atlantic thermohaline circulation in a coupled general circulation model: Unforced variations vs. forced changes. J. Clim. 18, 3270–3293.

Delworth, T.L., Dixon, K.W., 2000. Implications of the recent trend in the Arctic/North Atlantic Oscillation for the North Atlantic thermohaline circulation. J. Clim. 13, 3721–3727.

Deser, C., 2000. On the teleconnectivity of the Arctic oscillation. Geophys. Res. Lett. 27, 779–782.
Dickson, R.R., Lazier, J., Meincke, J., Rhines, P., Swift, J., 1996. Longterm coordinated changes in the convective activity of the North Atlantic. Prog. Oceanogr. 38, 241–295.
Dickson, R.R., Osborn, T.J., Hurrell, J.W., Meincke, J., Blindheim, J., Adlandsvik, B., Vinje, T., Alekseev, G., Maslowski, W., 2000. The Arctic Ocean response to the North Atlantic Oscillation. J. Clim. 13, 2671–2696.
Dickson, B., Yashayaev, I., Meincke, J., Turrel, B., Dye, S., Holfort, J., 2002. Rapid freshening of the deep North Atlantic ocean over the past four decades. Nature 416, 832–837.
Eden, C., Jung, T., 2001. North Atlantic interdecadal variability: Oceanic response to the North Atlantic oscillation (1865–1997). J. Clim. 14, 676–691.
Gent, P.R., 2001. Will the North Atlantic Ocean thermohaline circulation weaken during the 21st century? Geophys. Res. Lett. 28, 1023–1026.
Hall, M.M., Bryden, H.L., 1982. Direct estimates and mechanisms of ocean heat transport. Deep-Sea Res. 29, 339–359.
Hu, A., 2001. Changes in the Arctic and their impact on the oceanic Meridional Overturning Circulation, Ph.D. Dissertation (panoramix.rsmas.miami.edu/micom/micom-refs.html), University of Miami, 171pp.
Hu, A., Meehl, G.A., 2005. Reasons for a fresher northern North Atlantic in late 20th Century. Geophys. Res. Lett. 32, L11701. doi:10.1029/2005GL022900.
Hu, A., Meehl, G.A., Washington, W.M., Dai, A., 2004a. Response of the Atlantic thermohaline circulation to increased atmospheric CO_2 in a coupled model. J. Clim. 17, 4267–4279.
Hu, A., Meehl, G.A., Han, Weiqing, 2004b. Detecting thermohaline circulation changes from ocean properties in a coupled model. Geophys. Res. Lett. 31, L13204. doi:10.1029/2004GL020218.
Hughes, T.M.C., Weaver, A.J., 1994. Multiple equilibria of an asymmetric two-basin ocean model. J. Phys. Oceanogr. 24, 619–637.
Hurrell, J.W., 1995. Decadal Trends in the North Atlantic Oscillation: Regional Temperatures and Precipitation. Science 269, 676–679.
Josey, S.A., Marsh, R., 2005. Surface freshwater flux variability and recent freshening of the North Atlantic in the eastern subpolar gyre. J. Geophys. Res. 110, C05008. doi:10.1029/2004JC002521.
Kiehl, J.T., Hack, J.J., Bonan, G.B., Boville, B.A., Williamson, D.L., Rasch, P.J., 1998. The National Center for Atmospheric Research Community Climate Model: CCM3. J. Clim. 11, 1131–1150.
Levitus, S., Antonov, J., Boyer, T., 2005a. Warming of the world ocean, 1955-2003. Geophys. Res. Lett. 32, L02604. doi:10.1029/2004GL021592.
Levitus, S., Antonov, J.I., Boyer, T.P., Garcia, H.E., Locarnini, R.A., 2005b. Linear trends of zonally averaged thermosteric, halosteric, and total steric sea level for individual ocean basins and the world ocean, (1955–1959)–(1994–1998). Geophys. Res. Lett. 32, L16601. doi:10.1029/2005GL023761.
Lohmann, G., 2003. Atmospheric and oceanic freshwater transport during weak Atlantic overturning circulation. Tellus A 55, 438–449.
Marshall, J., Kushnir, Y., Battisti, D., Chang, P., Czaja, A., Dickson, R., Hurrell, J., McCartney, M., Saravanan, R., Visbeck, M., 2001. North Atlantic climate variability: phenomena, impacts and mechanisms. Int. J. Clim. 21, 1863–1898.
Maslanik, J.A., Serreze, M.C., Barry, R.G., 1996. Recent decreases in Arctic summer ice cover and linkages to atmospheric circulation anomalies. Geophys. Res. Lett. 23, 1677–1680.
McCartney, M.S., Talley, L.D., 1984. Warm-to-cold water conversion in the northern North Atlantic ocean. J. Phys. Oceanogr. 14, 922–935.
Meehl, G.A., Gent, P.R., Arblaster, J.M., Otto-Bliesner, B., Brady, E.C., Craig, A.P., 2001. Factors that affect amplitude of El Nino in global coupled models. Clim. Dyn. 17, 515–526.
Meehl, G.A., Washington, W.M., Wigley, T.M.L., Arblaster, J.M., Dai, A., 2003. Solar and Greenhouse Gas Forcing and Climate Response in the Twentieth Century. J. Clim. 16, 426–444.
Meehl, G.A., Washington, W.M., Ammann, C.M., Arblaster, J.M., Wigley, T.M.L., Tebaldi, C., 2004. Combinations of natural and anthropogenic forcings in twentieth-century climate. J. Climate 17, 3721–3727.
Mitchell, T.D., Carter, T.R., Jones, P.D., Hulme, M., New, M., 2004. A comprehensive set of high-resolution grids of monthly climate for Europe and the globe: the observed record (1901–2000) and 16 scenarios (2001–2100), Tyndall Centre Working Paper 55.
Parkinson, C.L., 2000. Variability of Arctic sea ice: The view from space, an 18-year record. Arctic 53, 341–358.
Parkinson, C.L., Cavalieri, D.J., Gloersen, P., Zwally, H.J., Comiso, J.C., 1999. Arctic sea ice extent, areas, and trends, 1978–1999. J. Geophys. Res. 104, 20837–20856.
Peterson, B.J., Holmes, R.M., McClelland, J.W., Vrsmarty, C.J., Lammers, R.B., Shiklomanov, A.I., Shiklomanov, I.A., Rahmstorf, S., 2002. Increasing river discharge to the Arctic Ocean. Science 298, 2171–2173.
Rahmstorf, S., 1996. On the freshwater forcing and transport of the Atlantic thermohaline circulation. Clim. Dyn. 12, 799–811.
Roemmich, D., Wunsch, C., 1985. Two transatlantic sections: Meridional circulation and heat flux in the subtropical North Atlantic Ocean. Deep-Sea Res. 32, 619–664.
Rothrock, D.A., Yu, Y., Maykut, G.A., 1999. Thinning of the Arctic sea-ice cover. Geophys. Res. Lett. 26, 3469–3472.
Ruhlemann, C., Mulitza, S., Muller, P.J., Wefer, G., Zahn, R., 1999. Warming of the tropical Atlantic Ocean and slowdown of the thermohaline circulation during the last deglaciation. Nature 402, 511–514.
Saenko, O.A., Weaver, A.J., Schmittner, A., 2003. Atlantic deep circulation controlled by freshening in the Southern Ocean. Geophys. Res. Lett. 30, 1734. doi:10.1029/2003GL017681.
Santer, B.D. et al., 2003a. Influence of satellite data uncertainties on the detection of externally-forced climate change. Science 300, 1280–1284.

Santer, B.D., Wehner, M.F., Wigley, T.M.L., Sausen, R., Meehl, G.A., Taylor, K.E., Ammann, C., Arblaster, J.M., Washington, W.M., Boyle, J.S., Bruggemann, W., 2003b. Contributions of anthropogenic and natural forcing to recent tropopause height changes. Science 301, 479–483.

Seidov, D., Haupt, B.J., 2003. Freshwater teleconnection and ocean thermohaline circulation. Geophys. Res. Lett. 30, 1329. doi:10.1029/2002GL016564.

Seidov, D., Haupt, B.J., 2005. How to run a minimalist's global ocean conveyor. Geophys. Res. Lett. 32, L07610. doi:10.1029/2005GL022559.

Smith, R.D., Kortas, S., Meltz, B., 1995. Curvilinear Coordinates for Global Ocean Models. LA-UR-95-1146. Los Alamos National Laboratory, Los Alamos, New Mexico, 38pp.

Smith, L.T., Chassignet, E.P., Bleck, R., 2000. The impact of lateral boundary conditions and horizontal resolution on North Atlantic water mass transformations and pathways in an isopycnic coordinate ocean model. J. Phys. Oceanogr. 30, 137–159.

Stocker, T.F., Wright, D.G., Broecker, W.S., 1992. The influence of high latitude surface forcing on the global thermohaline circulation. Paleoceanography 7, 529–541.

Stott, P.A., Tett, S.F.B., Jones, G.S., Allen, M.R., Mitchell, J.F.B., Jenkins, G.J., 2000. External control of 20th century temperature by natural and anthropogenic forcings. Science 290, 2133–2137.

Stouffer, R.J. et al., 2006. Investigating the causes of the response of the thermohaline circulation to past and future climate changes. J. Clim. 19, 1365–1387.

Thorpe, R.B., Gregory, J.M., Johns, T.C., Wood, R.A., Mitchell, J.F.B., 2001. Mechanisms determining the Atlantic thermohaline circulation response to greenhouse gas forcing in a non-flux-adjusted coupled climate model. J. Clim. 14, 3102–3116.

Toggweiler, J.R., Samuels, B., 1998. On the oceans large-scale circulation near the limit of no vertical mixing. J. Phys. Oceanogr. 28, 1832–1852.

Vinje, T., 2001. Fram Strait Ice fluxes and atmospheric circulation, 1950- 2000. J. Clim. 14, 3508–3517.

Vinnikov, K.Y., Robock, A., Stouffer, R.J., Walsh, J.E., Parkinson, C.L., Cavalier, D.J., Mitchell, J.F.B., Garrett, D., Zakharov, V.F., 1999. Global warming and Northern Hemisphere sea ice extent. Science 286, 1934–1937.

Walsh, J.E., Johnson, C.M., 1979. An analysis of arctic sea ice fluctuations, 195377. J. Phys. Oceanogr. 9, 580–591.

Washington, W.M., Weatherly, J.W., Meehl, G.A., Semtner Jr., A.J., Bettge, T.W., Craig, A.P., Strand Jr., W.G., Arblaster, J.M., Wayland, V.B., James, R., Zhang, Y., 2000. Parallel climate model (PCM) control and transient simulations. Clim. Dyn. 16, 755–774.

Wijffels, S.E., Schmitt, R.W., Bryden, H.L., 1992. Transport of freshwater by the oceans. J. Phys. Oceanogr. 22, 155–162.

Wu, P., Wood, R., Stott, P., 2004. Does the recent freshening trend in the North Atlantic indicate a weakening thermohaline circulation? Geophys. Res. Lett. 31, L02301. doi:10.1029/2003GL018584.

Xie, P.P., Arkin, P.A., 1996. Analysis of global monthly precipitation using gauge observations, satellite estimates, and numerical model predications. J. Clim. 9, 840–858.

Zhang, J.L., Hibler III, W.D., 1997. On an efficient numerical method for modeling sea ice dynamics. J. Geophys. Res. 102, 8691–8702.